HHS Public Access

Author manuscript

Cancer Cell. Author manuscript; available in PMC 2022 February 08.

Published in final edited form as:

Cancer Cell. 2021 February 08; 39(2): 193–208.e10. doi:10.1016/j.ccell.2020.11.005.

Immunogenic chemotherapy enhances recruitment of CAR-T cells to lung tumors and improves anti-tumor efficacy when combined with checkpoint blockade

Shivani Srivastava[1,*], **Scott N. Furlan**[1,2], **Carla A. Jaeger-Ruckstuhl**[1], **Megha Sarvothama**[1], **Carolina Berger**[1], **Kimberly S. Smythe**[1], **Sarah M. Garrison**[1], **Jennifer M. Specht**[1,3], **Sylvia M. Lee**[1,3], **Robert A. Amezquita**[4], **Valentin Voillet**[4], **Vishaka Muhunthan**[1], **Sushma Yechan-Gunja**[1], **Smitha P.S. Pillai**[5], **Christoph Rader**[6], **A. McGarry Houghton**[1], **Robert H. Pierce**[1], **Raphael Gottardo**[4], **David G. Maloney**[1,3], **Stanley R. Riddell**[1,3]

[1]Clinical Research Division, Fred Hutchinson Cancer Research Center, Seattle, WA

[2]Dept. of Pediatrics, University of Washington, Seattle, WA

[3]Dept. of Medicine, University of Washington, Seattle, WA

[4]Vaccine and Infections Disease Division, Fred Hutchinson Cancer Research Center, Seattle, WA

[5]Department of Comparative Medicine, Fred Hutchinson Cancer Research Center, Seattle, WA

[6]Department of Immunology and Microbiology, Scripps Research Institute, Jupiter, FL

Summary

Adoptive therapy using chimeric antigen receptor-modified T cells (CAR-T cells) is effective in hematologic but not epithelial malignancies, which cause the greatest mortality. In breast and lung cancer patients, CAR-T cells targeting the tumor-associated antigen receptor tyrosine kinase-like orphan receptor 1 (ROR1) infiltrate tumors poorly and become dysfunctional. To test strategies for enhancing efficacy, we adapted the *Kras*$^{LSL\text{-}G12D/+}$;*p53*$^{f/f}$ autochthonous model of lung

[*]**Lead contact and corresponding author:** Shivani Srivastava, Fred Hutchinson Cancer Research Center, 1201 Eastlake Ave E, S3-213, Seattle, WA 98102. Phone: (206) 667-5103; ssrivas2@fredhutch.org.

Author Contributions

S.S. and S.R.R. conceived the study, designed experiments, and wrote the manuscript. S.S. performed experiments, analyzed the data, and interpreted results. C.A.J., V.M., J.M.S., S.M.L., C.B., and D.G.M collected and analyzed patient data. S.N.F., V.V., R.A.A., and R.G. performed analysis of single-cell and bulk RNA sequencing data. M.S., S.G. and S.Y.G. performed experiments. K.S.S., S.P.S.G., R.H.P. performed and analyzed immunohistochemistry staining. S.S. and A.M.S. performed intratracheal injection of Cre lentivirus. C.R. provided R12 and 2A2 antibodies for development of clinical and murine ROR1 CAR-T cells.

Declaration of Interests

S.S. and S.R.R. are inventors on a patent ("Immunogenic chemotherapy markedly enhances the efficacy of ROR1 CAR T cells in lung adenocarcinoma"; PCT/US2018/049812) filed by Fred Hutchinson Cancer Research Center and licensed by Lyell Immunopharma. S.S. holds equity and has served as a consultant for Lyell Immunopharma. D.G.M. has received research funding from Kite Pharma, Juno Therapeutics, and Celgene, and has served on advisory boards for Kite Pharma, Gilead, Genentech, Novartis, and Eureka Therapeutics. S.R.R. was a founder, has served as an advisor, and has patents licensed to Juno Therapeutics; is a founder of and holds equity in Lyell Immunopharma; and has served on the advisory boards for Adaptive Biotechnologies and Nohla. C.R. is named inventor on U.S. Patent 9,758,586 claiming anti-ROR1 monoclonal antibodies R11 and R12 and is on the advisory board of NBE-Therapeutics. No potential conflicts of interest were disclosed by the other authors.

adenocarcinoma to express the CAR target ROR1. Murine ROR1 CAR-T cells transferred after lymphodepletion with cyclophosphamide (Cy) transiently control tumor growth but infiltrate tumors poorly and lose function, similar to patients. Adding oxaliplatin (Ox) to the lymphodepletion regimen activates tumor macrophages to express T cell-recruiting chemokines, resulting in improved CAR-T cell infiltration, remodeling of the tumor microenvironment, and increased tumor sensitivity to anti-PD-L1. Combination therapy with Ox/Cy and anti-PD-L1 synergistically improves CAR-T mediated tumor control and survival, providing a strategy to improve CAR-T cell efficacy in the clinic.

Graphical Abstract

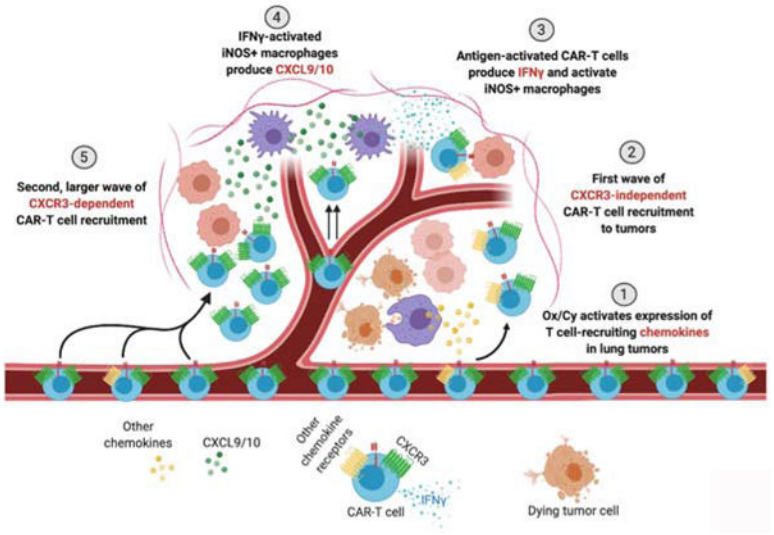

eTOC

Srivastava *et al.* demonstrate that adding oxaliplatin to the lymphodepletion regimen given before CAR-T cell infusion activates lung tumor macrophages to produce T cell-recruiting chemokines. This results in improved CAR-T cell infiltration, tumor remodeling, and response to checkpoint blockade, providing a strategy to improve CAR-T cell efficacy in the clinic.

Keywords

CAR-T cells; ROR1; KP; lung adenocarcinoma; oxaliplatin; immunogenic cell death; alveolar macrophage; CXCR6; CXCR3

Introduction

Adoptive cell therapy with tumor-reactive T cells (ACT) can be effective for some cancers (Guedan et al., 2019, Rosenberg and Restifo, 2015). ACT using autologous T cells modified by gene transfer to express a chimeric antigen receptor (CAR) specific for the CD19 molecule present on both normal B cells and B cell malignancies has shown remarkable success in leukemia and lymphoma (Kochenderfer and Rosenberg, 2013). However, achieving efficacy with T cells engineered with receptors specific for antigens on epithelial

cancers, which account for 80 to 90 percent of all cancers, has proven challenging (Srivastava and Riddell, 2018).

There are several barriers that may underlie the relative lack of efficacy of ACT in solid tumors compared with hematological cancers (Srivastava and Riddell, 2018). Solid tumors typically reside in non-lymphoid tissues where T cells may not traffic efficiently without appropriate inflammatory signals to recruit them. Moreover, solid tumors can recruit immunosuppressive cells, release immunosuppressive molecules, and inhibit T cells directly through expression of ligands for inhibitory receptors like PD-1. Understanding which barriers interfere most with T cell efficacy *in vivo* and developing strategies to overcome these obstacles is necessary to achieve reproducible antitumor activity with CAR-T cells.

We sought to develop a model that faithfully mimics tumor development and the tumor microenvironment (TME) found in human malignancies to guide clinical strategies for improving the efficacy of T cells in solid tumors. Studies evaluating antitumor activity of CAR-T cells *in vivo* have relied heavily on rapidly progressive transplantable human tumor xenografts in immunodeficient *NOD/scid/*$\gamma c^{-/-}$ (NSG) mice that lack T cells, NK cells, and B cells and do not emulate the initiation, progression, and complex TME of human cancer (DuPage and Jacks, 2013). Likewise, most immune-competent transplantable mouse models implant tumor cells in foreign anatomical sites. Transplanted tumors grow rapidly, do not co-evolve naturally with host immunity, and can be artificially immunogenic due to the implantation process (DuPage et al., 2011, Garbe et al., 2006, DuPage and Jacks, 2013).

An alternative to transplantable models is to induce malignant transformation in normal cells *in situ* by introducing defined genetic events. Genetically-engineered mouse (GEM) models recapitulate tumor initiation, progression, and the genetic and histopathological characteristics of human cancers (DuPage and Jacks, 2013). *Kras*$^{LSL\text{-}G12D/+}$*;p53*$^{f/f}$ (KP) mice are a model of lung adenocarcinoma, in which intratracheal injection of a Cre-expressing lentivirus initiates p53 deletion and Kras^{G12D} activation in lung airway cells, resulting in growth of tumors that histopathologically resemble human lung cancer (DuPage et al., 2011, DuPage et al., 2009).

We modified the KP model by introducing a receptor tyrosine kinase-like orphan receptor 1 (ROR1) transgene into the Cre lentivirus used to induce tumors (hereafter termed KP^{ROR1} mice). ROR1 is being investigated in a clinical trial as a target for CAR-T cells due to its high expression in a subset of non-small cell lung cancer (NSCLC) and triple-negative breast cancer (TNBC). Similar to what we observed in patients, murine ROR1 CAR-T cells infiltrate KP^{ROR1} tumors poorly and have only transient antitumor activity. Here, we use the KP^{ROR1} model to identify and evaluate strategies to enhance CAR-T cell trafficking to tumors to improve treatment efficacy.

Results

ROR1 CAR-T cells infiltrate tumors poorly and become dysfunctional in patients with ROR1$^+$ TNBC and NSCLC

We previously developed CARs that redirect T cell specificity to ROR1$^+$ human tumor cells *in vitro* and were effective in human tumor xenograft models (Hudecek et al., 2013, Hudecek et al., 2010). Though ROR1 is also expressed in some normal tissues, it remains absent from vital adult human tissues (Balakrishnan et al., 2017, Hudecek et al., 2010), and ROR1 CAR-T cells were safe and functional in non-human primates (NHP) (Berger et al., 2015). Based on these data, a clinical trial (NCT02706392) in patients with ROR1$^+$ TNBC and NSCLC is being conducted at our center. Patients are treated with cyclophosphamide (Cy) and fludarabine (Flu) for lymphodepletion prior to infusion with autologous CD8$^+$ and CD4$^+$ T cells engineered to co-express a ROR1 CAR carrying 4–1BB and CD3ζ signaling domains and truncated EGFR (tEGFR) as a transduction marker (Table S1, Fig. 1A). We observed robust CAR-T cell expansion in the peripheral blood of three treated patients without toxicity to normal tissues (Fig. 1B). At the peak of expansion in peripheral blood, ROR1 CAR-T cells upregulated multiple inhibitory receptors and lost the ability to produce IFNγ, TNFα, and GM-CSF upon restimulation *ex vivo* compared with CAR-T cells in the infusion product (Fig. 1C, 1D). A tumor biopsy obtained post-treatment from one patient showed few infiltrating ROR1 CAR-T cells by flow cytometry, indicating that CAR-T cells failed to accumulate or persist in ROR1$^+$ tumors (Fig. 1E). Consistent with poor infiltration, tumor regression was not observed in these patients. These data suggest that lack of sustained CAR-T cell infiltration at tumor sites and rapid dysfunction are barriers to efficacy in solid tumors.

Development of a GEM model of ROR1$^+$ lung cancer for CAR-T cell therapy

We sought to develop animal models to evaluate strategies to overcome the barriers to CAR-T cells in solid tumors. We found that ROR1 CAR-T cells easily infiltrated lung tumors established by transplanting ROR1$^+$ tumor cell lines derived from KP GEM mice, which was distinct from what we observed in patients (Fig. S1A,B). To more closely mimic human lung cancer, we engineered a lentivirus to induce ROR1$^+$ tumors in KP mice by co-expressing Cre recombinase, firefly luciferase (ffluc) and human ROR1 (hROR1) and validated their expression *in vitro* using Cre-reporter cell lines (Sanchez-Rivera et al., 2014) (Fig. S2A–C). Including ffluc allowed us to validate expression of the Cre-ffluc-hROR1 transgene in lung cells after intratracheal delivery using non-invasive bioluminescent imaging (BLI). We chose to use hROR1 (97% identity with mROR1) because murine ROR1 (mROR1) is expressed in bone marrow stromal cells and leads to toxicity when mROR1-targeted CAR-T cells are administered after intensive lymphodepletion (Srivastava et al., 2019). To target hROR1, we used a ROR1 CAR derived from the murine 2A2 single chain variable fragment (scFv) that recognizes a similar epitope on hROR1 as the R12 CAR used in the clinical trial and does not cross-react with mROR1 (Hudecek et al., 2013, Yang et al., 2011).

KP mice infected intratracheally with Cre-ffluc (KP mice) or Cre-ffluc-hROR1 lentiviruses (KP^{ROR1} mice) developed lung tumors visible by magnetic resonance imaging (MRI) and BLI at 9–12 weeks post-infection (Fig. S2D–E). Tumors in KP^{ROR1}, but not KP, mice

expressed high levels of ROR1 comparable to endogenous ROR1 in a human breast cancer cell line (Fig. S2F–G). The frequency and phenotype of tumor-infiltrating lymphocytes and myeloid cells did not differ in KP or KP^{ROR1} tumors (Fig. S3A–D), suggesting immunity was not enhanced by the few disparate sequences in hROR1.

ROR1 CAR-T cells modestly control tumor growth in KP^{ROR1} mice

The function and specificity of a 2A2 ROR1 CAR was previously described and comparable *in vitro* to the R12 CAR used in the clinic (Hudecek et al., 2013). To adapt the 2A2 CAR for use in mouse T cells, we replaced human 4–1BB and CD3ζ with murine sequences and co-expressed a truncated murine CD19 fused to GFP (tCD19-GFP) transduction marker downstream of a P2A ribosomal skip element to allow *in vivo* tracking of CAR-T cells. Control T cells were engineered to express the tCD19-GFP transduction marker alone.

To evaluate antitumor effects of ROR1 CAR-T cells in KP^{ROR1} mice, we treated tumor-bearing KP^{ROR1} mice with cyclophosphamide (Cy) for lymphodepletion and infused ROR1 CAR-T cells or control T cells every three weeks (Fig. 2A). ROR1 CAR-T cells significantly reduced tumor growth compared to control T cells for the first 6 weeks of treatment (Fig. 2B). All tumors, however, eventually progressed and survival was not significantly improved by this treatment regimen (Fig. 2C).

To assess the phenotype of CAR-T cells *in situ*, we analyzed lungs from wild-type (WT) and tumor-bearing KP^{ROR1} mice 10 days after the second infusion of T cells, when CAR-T cells peaked in expansion in the blood (Fig. 2D), and used a PE-antibody labeling method to exclude contaminating cells from the lung vasculature (Pereira et al., 2009, Anderson et al., 2014). ROR1 CAR-T cells were enriched ~2-fold compared to control T cells among PE-negative non-vascular CD8$^+$ T cells in KP^{ROR1} lungs but not in WT lungs (Fig. 2E). CAR-T cells from tumor-bearing lungs upregulated inhibitory receptors like PD-1, LAG-3, and TIM-3 and produced lower levels of IFNγ and TNFα upon re-stimulation *ex vivo* compared to both control T cells and CAR-T cells in non-tumor bearing lungs (Fig. 2E, 2F). Consistent with the rapid acquisition of CAR-T cell dysfunction, tumors that progressed in CAR-T cell-treated mice maintained similar levels of ROR1 expression as in control T cell-treated mice, indicating that antigen loss was not the mechanism of tumor escape (Fig. 2G, 2H). ROR1 CAR-T cells, thus, mediate modest but incomplete control of tumor growth in KP^{ROR1} mice.

ROR1 CAR-T cell do not efficiently infiltrate all ROR1$^+$ tumors

All tumor nodules progressed in control T cell-treated KP^{ROR1} mice, whereas tumors in ROR1 CAR-T cell-treated mice showed mixed responses, with a fraction of nodules regressing, remaining stable, or progressing in the same mouse (Fig. 3A). Incomplete response to immunotherapy is common in patients and in animal models and can correlate with the degree of T cell infiltration (Jiang et al., 2018, Topalian et al., 2012, Li et al., 2018). To determine whether differences in T cell infiltration underlay the heterogeneity in tumor nodule growth, we treated tumor-bearing KP^{ROR1} mice with Cy and control or CAR-T cells every 3 weeks and analyzed lungs by immunohistochemistry (IHC) 10 days after the second infusion of T cells. Tumors from each lung were scored for absence of T cells (<5% CD3$^+$ cells), peripheral/stromal, or intratumoral localization of CD3$^+$ T cells. Most tumors in

control T cell-treated mice were devoid of T cells or localized to the periphery/stroma, with < 5% of tumors having intratumoral T cells (Fig. 3B). Although a larger fraction of tumors nodules showed intratumoral infiltration after CAR-T cell treatment, more than half of tumor nodules in CAR-T cell-treated mice were devoid of T cells (Fig. 3B).

We hypothesized that poor T cell infiltration in KP^{ROR1} tumors may be due to insufficient local production of T cell-recruiting chemokines. Although CAR-T cells in the circulation highly expressed CXCR3 and to a lesser degree CXCR6 and CCR5 (Fig. 3C), tumor nodules excised from untreated KP^{ROR1} mice showed low transcript levels of the CXCR3 ligands *Cxcl9, Cxcl10*, and *Cxcl11*, the CCR5 ligand *Ccl5*, or the CXCR6 ligand *Cxcl16* (Fig. 3D). By contrast, *Cxcl5*, which is involved in recruitment of $CXCR2^+$ neutrophils, and *Cxcl12*, which mediates cross-talk between tumor and $CXCR4^+$ stroma (Guo et al., 2016), were the most highly expressed chemokines detected in KP^{ROR1} tumors. ROR1 CAR-T cells, thus, failed to traffic appreciably to most KP^{ROR1} lung tumors likely due to insufficient local production of T cell-recruiting chemokines, and limited infiltration may in part underlie the susceptibility of CAR-T cells to exhaustion and eventual outgrowth of tumors.

Ox/Cy enhances chemokine expression and accumulation of CAR-T cells in KP^{ROR1} lung tumors

Because of the lack of signals for recruiting T cells into KP^{ROR1} tumors, we asked whether activation of immunogenic cell death (ICD) in lung tumors might induce expression of molecules that promote CAR-T cell infiltration into tumors. Administration of oxaliplatin and cyclophosphamide (Ox/Cy) together has been shown to induce ICD, resulting in release of pro-inflammatory mediators from dying cells, innate immune cell activation, T cell priming and migration to tumors, and improved tumor responses to checkpoint blockade (Pfirschke et al., 2016). Although CAR-T cells do not require interactions with antigen-presenting cells for activation, we hypothesized that alterations induced in the TME by ICD, such as production of CXCR3 ligands and activation of the endothelium, might lead to enhanced CAR-T cell infiltration.

We treated KP^{ROR1} tumor bearing mice with three weekly injections of Ox/Cy or vehicle, at a dose and frequency previously shown to induce ICD (Pfirschke et al., 2016). Six hours after the last Ox/Cy dose, individual lung tumors were excised, pooled, and gene signatures analyzed by RNA sequencing (RNA-seq) (Data S1). Ox/Cy treatment resulted in differential expression of 418 genes, 287 of which were upregulated and 131 downregulated (Fig. 4A). Genes involved in inflammation of the endothelium (*Sele, Selp*), activation of innate immune cells (*Tnfsf4*, *Cd40, Tnfsf11, Cd80)*, and interferon signaling (*Irf7, Isg15*) were significantly upregulated, suggesting an overall shift in the TME towards a pro-inflammatory state. Gene-set enrichment analysis demonstrated that, among genes upregulated by Ox/Cy, cytokine-cytokine receptor interaction, chemokine signaling, and JAK/STAT signaling genesets were significantly enriched (Fig. 4B). Genes involved in T cell chemotaxis were among the leading-edge genes that contributed most to enrichment of the cytokine signaling pathway (Fig. 4C). Although all Ox/Cy-treated tumors upregulated genes involved in cytokine and chemokine signaling, stronger upregulation of these genes occurred

in smaller tumors (<5 mm in diameter) compared to larger tumors (>5 mm in diameter), indicating heterogeneity in the response to Ox/Cy.

To examine whether the changes to the TME induced by Ox/Cy were sufficient to improve CAR-T infiltration into KP^{ROR1} tumors, we pre-treated tumor-bearing KP^{ROR1} mice with Ox/Cy or vehicle as before (Fig. 4D). Both Ox/Cy- and vehicle-treated mice received a lymphodepleting dose of Cy 6 hours prior to infusion with control or ROR1 CAR-T cells. Ox/Cy significantly enhanced CAR-T cell accumulation in tumors, but not spleens, compared to vehicle by 10 days post-transfer (Fig. 4E). Notably, the level of lymphodepletion induced prior to T cell transfer was not altered by adding Ox/Cy to the treatment regimen (Fig. 4F), indicating that greater lymphopenia was not the reason for enhanced CAR-T cell accumulation in Ox/Cy-treated tumors.

Ox/Cy activates expression of T cell-recruiting chemokines by tumor macrophages

To resolve how Ox/Cy altered the phenotype of the TME to permit greater CAR-T cell entry, we treated tumor-bearing KP^{ROR1} mice with Ox/Cy or vehicle, administered a lymphodepleting dose of Cy to all mice, and transferred ROR1 CAR-T cells as before (Fig. 4D). We excised lung tumors for single cell RNA sequencing (scRNA-seq) at two time points: 6 hours after injection of Ox/Cy (D0, pre-CAR-T cell infusion) or 10 days after CAR-T cell infusion (D10). We analyzed the scRNA-seq profiles of cells from tumors at each time point and of the $CD8^+$ CAR-T cell infusion product (Data S2). Unsupervised clustering analysis revealed populations that we identified based on lineage and phenotypic marker expression as tumor/epithelial cells (*Epcam*), endothelial cells (*Pecam1*), B cells (*Cd19*), NK cells (*Klrb1c*), T cells (*Cd3d*), the CAR-T cell infusion product (CAR transgene), neutrophils (*Cxcr2, S100a9*), red blood cells (*Hba-a1*), plasmacytoid dendritic cells (DCs) (*Siglech*), plasma B cells (*Tnfrsf17*), and mononuclear phagocytes (MNP) that shared variable expression of macrophage, DC, and monocyte markers (e.g. *Cd68*, *Itgax*, *Itgam*, *Adgre1*) (Fig. 5A, Fig. S4A).

The T cell cluster was comprised primarily of cells from mice treated with Ox/Cy, both pre- and post-CAR-T cell infusion (Fig. 5B, 5C). CAR expression was limited to T cells from the infusion product and to cells from tumors at D10 after Ox/Cy (Fig. 5D), consistent with our data showing enhanced CAR-T cell infiltration into Ox/Cy-treated tumors (Fig. 4E). Ox/Cy also increased the frequency of endogenous T cells in tumors on D0 (Fig. 5B, 5C), but these T cells did not express activation-associated transcripts, suggesting they were not tumor-specific (Fig. 5D, Fig. S4B). Activation-associated transcripts were expressed in the cluster associated with CAR-T cells at D10 after Ox/Cy and were not present in the infusion product (Fig. 5D, Fig. S4B), suggesting that cells were activated *in vivo*. Likewise, the NK cell cluster was preferentially comprised of cells from mice treated with Ox/Cy and expressed transcripts associated with effector function (*Ifng*, *Gzmb*) (Fig. 5C, Fig. S4B).

Ox/Cy also induced major changes in the cluster associated with MNP. We were able to divide the MNP cluster into three broad cell types clearly identified as macrophages, DCs, and monocytes and validated these annotations using a neural network trained on published scRNA-seq data (Fig. S4A, S5A, S5B) (Zilionis et al., 2019). Within this embedding, the macrophages, in particular, self-aggregated into four separate sub-clusters (Fig. 6A–C),

which showed a striking enrichment in cells from different treatment groups (Fig. 6D). We hypothesized that this transcriptional patterning was reflective of the various states of macrophage activation induced by treatment with Ox/Cy and/or CAR-T cells. The four sub-clusters could be distinguished by expression of the alveolar macrophage (AM) marker *Siglecf*, the "M2"-like tissue macrophage marker *Mrc1*, and the pro-inflammatory "M1"-state marker *Nos2* (Fig. 6E) (MacMicking et al., 1997, Mantovani et al., 2002). Clusters 3 and 4 represented AM in untreated tumors at D0, as these clusters were enriched for AM genesets and were identified as AMs by the neural network described above (Fig. 6E, 6F; Fig S6B) (Zilionis et al., 2019). Cluster 2, which consisted exclusively of cells derived from tumors excised from mice 6 hr after Ox/Cy, showed enrichment of macrophage activation, cytokine and chemokine expression, and TLR signaling genesets compared to the "AM" clusters (Fig. 6F, 6G), suggesting tumor macrophages were activated early after Ox/Cy.

Cluster 1, by contrast, uniquely expressed *Nos2* and exhibited a strong IFNγ response signature (Fig. 6E, 6F), with enrichment of antigen presentation, cytokine expression, and chemokine signaling genesets relative to clusters 2 and 3 (Fig. 6G). We confirmed an increase in iNOS^{+} tumor macrophages 10 days after treatment with Ox/Cy and CAR-T cells, and this accumulation depended on IFNγ production by CAR-T cells (Fig. 6H–I). Interestingly, although WT and IFNγ$^{-/-}$ CAR-T cells accumulated at similar levels in spleens of Ox/Cy-treated KP^{ROR1} mice, recruitment of IFNγ$^{-/-}$ CAR-T cells to tumors was significantly reduced and correlated with a decrease in iNOS^{+} macrophages. As *Nos2*-expressing Cluster 1 macrophages were the major source of multiple T cell-recruiting chemokines, including *Cxcl9*, *Cxcl10*, *Ccl5*, and *Cxcl16* (Fig. 6J), these data suggest that IFNγ produced by CAR-T cells activates iNOS^{+} macrophages, which provide a source of chemokines that facilitate further recruitment of CAR-T cells to tumors.

We hypothesized that Ox/Cy-induced chemokine expression in tumor macrophages may facilitate CAR-T cell recruitment. Clusters 3 and 4 did not express substantial levels of *Ccl5*, *Cxcl16*, *Cxcl9*, or *Cxcl10* (Fig. 6J). However, cluster 2, representing cells from tumors 6 hr after Ox/Cy treatment, selectively upregulated the CXCR6-ligand *Cxcl16* (Fig. 6J), for which macrophages and DCs were the dominant source by scRNA-seq (Fig. S6). In contrast, the "M1"-like macrophage cluster 1 upregulated CXCR3-ligands *Cxcl9* and *Cxcl10*, the CCR5-ligand *Ccl5*, and the CXCR6-ligand *Cxcl16* relative to the other macrophage clusters. Cluster 1 macrophages were the dominant source of *Cxcl9* and *Cxcl10* relative to all other cell populations (Fig. S6).

Based on our single cell RNA-seq data showing sequential upregulation of *Cxcl16* and then *Cxcl9/Cxcl10* after Ox/Cy, we hypothesized that different chemokines may mediate early versus late recruitment of CAR-T cells into tumors. To test this, we generated ROR1 CAR-T cells from wild-type (WT), *Cxcr3*$^{-/-}$, *Cxcr6*$^{-/-}$, or *Ccr5*$^{-/-}$ mice. We pre-treated tumor-bearing KP^{ROR1} mice with Ox/Cy as before, with the final dose incorporating a lymphodepleting dose of Cy and given 6 hours before CAR-T cell infusion. As a control, KP^{ROR1} mice were treated with Cy alone 6 hours before T cell transfer. We then infused KP^{ROR1} mice with a 1:1 mix of WT and chemokine receptor-deficient ("KO", *Cxcr3*$^{-/-}$, *Cxcr6*$^{-/-}$, or *Ccr5*$^{-/-}$) ROR1 CAR-T cells. WT and KO CAR-T cells were present at similar frequencies in spleens, indicating that deficiency in each receptor did not impact

homeostatic proliferation or ability of the CAR-T cells to engraft (Fig. 6J). At day 2 post-transfer, Ox/Cy enhanced accumulation of CAR-T cells in tumors excised from KP^{ROR1} mice, and this accumulation was partially CXCR6- and CCR5-dependent, as *Cxcr6*$^{-/-}$ and *Ccr5*$^{-/-}$ CAR-T cells showed poorer tumor infiltration compared to their WT counterparts (Fig. 6K). Consistent with low expression of CXCR3 ligands in tumor macrophages early after Ox/Cy, infiltration of CAR-T cells into tumors on day 2 was completely CXCR3-independent. By contrast, accumulation of WT CAR-T cells by day 10 after Ox/Cy depended completely on CXCR3 but not CCR5 or CXCR6 (Fig. 6K), likely facilitated by the high expression of the CXCR3 ligands *Cxcl9* and *Cxcl10* by cluster 1 macrophages at this time point. Ox/Cy, thus, initially activates expression of multiple T cell-recruiting chemokines that facilitate early entry of CAR-T cells into tumors, a process which is partially dependent on CXCR6 and CCR5. Infiltration of CAR-T cells into tumors leads to further activation of "M1"-like $iNOS^+$ tumor macrophages to produce *Cxcl9* and *Cxcl10*, resulting in CXCR3-dependent recruitment of CAR-T cells.

Ox/Cy-enhanced CAR-T cell infiltration sensitizes tumors to anti-PD-L1

Although Ox/Cy enhanced CAR-T cell migration to tumors, we anticipated that additional inhibitory mechanisms may impede anti-tumor activity. Tumor-infiltrating CAR-T cells highly expressed PD-1 (Fig. 2E), and PD-L1 (*Cd274*) transcripts were highly expressed in the M1 macrophage cluster relative to other cell populations identified (Fig. 7A, 7B), consistent with the IFNγ signature in this cluster (Fig. 6F). Surface PD-L1 increased significantly on tumor macrophages only after treatment with both CAR-T cells and Ox/Cy (Fig. 7C). Infiltration of CAR-T cells into Ox/Cy-treated tumors, thus, induced upregulation of PD-L1 on tumor macrophages, which could inhibit the function of $PD\text{-}1^+$ CAR-T cells. Although Ox/Cy increased the frequency of CAR-T cells in tumors (Fig. 7D), control of tumor growth was not improved (Fig. 7E).

To examine whether disruption of the PD-1/PD-L1 axis could improve efficacy of CAR-T cells in Ox/Cy-treated tumors, we pre-treated tumor-bearing KP^{ROR1} mice as before with Ox/Cy or vehicle, infused control or ROR1 CAR-T cells, and treated mice with anti-PD-L1 or vehicle beginning one day after infusion. We continued treating mice every 3 weeks with Cy or Ox/Cy for lymphodepletion and control or CAR-T cells. Anti-PD-L1 treatment did not increase the frequency of CAR-T cells in the tumor or improve tumor control (Fig. 7D, 7E). By contrast, the combination of Ox/Cy, CAR-T cells and anti-PD-L1 led to a significant increase in CAR-T cell accumulation and tumor control compared to CAR-T cell-treated mice that received either Ox/Cy or anti-PD-L1 alone (Fig. 7D, 7E). Thus, improved tumor control was only achieved by synergistic enhancement of CAR-T cell infiltration with Ox/Cy and CAR-T cell function with anti-PD-L1.

We further characterized the tumor response to our optimized treatment regimen of Ox/Cy, anti-PD-L1 and ROR1 CAR-T cell infusion. All tumor nodules progressed in mice receiving control T cells alone or in combination with Ox/Cy and/or anti-PD-L1 (Fig. 8A, 8B). A small fraction of tumors regressed in mice treated with ROR1 CAR-T cells as observed previously. However, mice receiving Ox/Cy, CAR-T cells and anti-PD-L1 showed regression of a majority of tumor nodules, and those that persisted grew at a slower rate (Fig. 8A, 8B).

Ox/Cy and anti-PD-L1 treatment significantly improved the density of $CD3^+$ T cells in tumors in CAR-T cell-treated mice but not in control T cell-treated mice, with more tumors showing intratumoral T cell localization (Fig. 8C, 8D). CAR-T cells in Ox/Cy-treated mice had reduced expression of LAG-3 and TIM-3 and increased production of IFNγ and TNFα upon re-stimulation *ex vivo* compared with Cy-treated mice, indicating improved CAR-T cell function in the TME (Fig. 8E, 8F). Correspondingly, Ox/Cy and anti-PD-L1 treatment significantly improved CAR-T cell-mediated survival of KP^{ROR1} mice but not in mice receiving control T cells (Fig. 8G).

To determine whether the effects of Ox/Cy on CAR-T cell activity extended to other cancers, we also examined this treatment strategy in the 4T1 model of TNBC, a malignancy which also highly expresses ROR1. Ox/Cy significantly enhanced tumor control by ROR1 CAR-T cells, but not by control T cells (Fig. S7). The addition of anti-PD-L1 was not required to observe the beneficial effects of Ox/Cy preconditioning on CAR-T cell efficacy, possibly due to the transplantable nature of this model, which may make it more susceptible to CAR-T cells than the KP model. Immunogenic chemotherapy, thus, dramatically improves CAR-T cell-mediated control of both $ROR1^+$ breast and lung tumors.

Ox/Cy and CAR-T cells improve intratumoral T cell infiltration and induce clinical responses in a patient with $ROR1^+$ TNBC

To examine whether Ox/Cy induced similar responses in patients, we modified our clinical protocol to administer Ox/Cy for lymphodepletion. We obtained pre- and post-treatment tumor biopsies from one refractory TNBC patient who received Ox/Cy. ROR1 CAR-T cells were detected in the blood after T cell infusion and this patient exhibited stable disease at day 2, and achieved a partial remission by RECIST criteria lasting >7 months after a second CAR-T cell infusion with Cy/Flu lymphodepletion (Fig. S8A). Although we were unable to evaluate the frequency of CAR-T cells in the core needle biopsies, we observed an increase in $CD3^+$ T cells and a reduction in $CD206^+/CD163^+$ “M2”-like macrophages at day 18 post-Ox/Cy and CAR-T infusion compared to pre-treatment, consistent with our results in the KP model. Residual tumor was re-biopsied on day 203 during the partial remission, and showed a further increase in intratumoral $CD3^+$ T cells and decline in $CD206^+$ macrophages, again consistent with our results demonstrating progressive remodeling of the TME over time (Fig. S8B–C). These data indicate that Ox/Cy favorably remodels the TME to promote T cell infiltration and suggest that this lymphodepletion regimen can substantially improve clinical responses to CAR-T cell therapy.

Discussion

CAR-T cells are effective for blood cancers but have had limited success in common epithelial cancers. Poor infiltration into tumor sites and loss of function of T cells have been identified as barriers to efficacy (Lanitis et al., 2017, Srivastava and Riddell, 2018), and we encountered these obstacles in a clinical trial using CAR-T cells to target ROR1 in patients with human NSCLC and TNBC. Using a GEM model of NSCLC that mimics the initiation, progression, and therapeutic response of human lung cancer, we show that CAR-T cell migration to tumors can be improved by pre-treatment with Ox/Cy chemotherapy and that

this regimen improves survival when combined with anti-PD-L1 checkpoint blockade. Mechanistically, we demonstrate that Ox/Cy activates multiple pro-inflammatory pathways, including expression of T cell-recruiting chemokines by multiple cell types in the TME, which facilitates initial recruitment of CAR-T cells to tumors that is partially dependent on CCR5 and CXCR6 expression. Infiltrating CAR-T cells produce IFNγ and remodel the TME to activate M1 macrophages expressing the CXCR3 ligands *Cxcl9* and *Cxcl10*, initiating a positive feedback loop supporting further CXCR3-dependent CAR-T cell recruitment to tumors. Ox/Cy enhanced CAR-T cell infiltration increased tumor sensitivity to checkpoint blockade, demonstrating that improving both CAR-T cell migration into and function within tumors is necessary to improve survival.

Trafficking of T cells to solid tumors is often limited by the poor production of T cell-recruiting chemokines (Harlin et al., 2009). While this issue can be bypassed by delivering CAR-T cells directly to the tumor (Brown et al., 2016, Brown et al., 2015, Adusumilli et al., 2014, Priceman et al., 2018, van Schalkwyk et al., 2013), this strategy is not feasible for most epithelial cancers which can metastasize widely. Homing of CAR-T cells to tumors can be improved by engineering them to express chemokine receptors that are specific for chemokines naturally overproduced by some tumors (Jin et al., 2019, Liu et al., 2020, Peng et al., 2010, Whilding et al., 2019, Craddock et al., 2010, Moon et al., 2011, Stasi et al., 2009), or by using oncolytic viruses and STING agonists to induce tumors to express chemokines that attract activated T cells (Nishio and Dotti, 2015, Ribas et al., 2017, Woo et al., 2014). Here, we demonstrate that immunogenic chemotherapy activates tumor macrophages to produce chemokines that facilitate recruitment of CAR-T cells to lung tumors. A recent study demonstrated that constitutive CCL5 production by human tumor cells recruited an initial wave of T cells that produce IFNγ upon antigen recognition and activate macrophages and DCs to secrete CXCL9, recruiting a second wave of $CXCR3^+$ T cells (Dangaj et al., 2019). Our data suggest an analogous circuit involving sequential expression of *Ccl5* and *Cxcl16* followed by *Cxcl9* and *Cxcl10* that governs successful trafficking of infused CAR-T cells to lung tumors. Although peak CAR-T cell infiltration was strongly CXCR3-dependent, early infiltration of CAR-T cells was surprisingly CXCR3-independent, indicating that the signals that mediate early versus peak CAR-T cell recruitment were distinct. Our data indicate that early infiltration is at least partially dependent on CXCR6 and CCR5, but it is likely that a number of mechanisms (e.g. activated endothelium, other chemokines) may facilitate initial CAR-T cell entry into tumors after Ox/Cy, and further work is needed to identify these signals and how expression of various chemokines are temporally regulated in the TME.

Analysis of tumors using scRNA-seq suggested that Ox/Cy improves CAR-T cell recruitment to tumors by modulation of macrophages in the TME. The macrophage compartment in untreated, progressing KP tumors was predominantly comprised of AMs expressing pro-tumor-associated transcripts, including those for suppressive cytokines (*Tgfb1*, *Il10*) and osteopontin (*Spp1*), which is overexpressed in human lung cancer and associated with poor prognosis (Rud et al., 2013). Our data suggest that Ox/Cy causes a rapid shift in the tumor macrophage compartment towards an activated phenotype characterized by enhanced TLR signaling, cytokine production, and chemokine signaling. How tumor macrophages are activated following treatment with Ox/Cy requires further

study. ICD is known to result in release of HMGB1 and calreticulin from dying cells that can act as TLR4 agonists (Krysko et al., 2012), and Ox/Cy induction of ICD is TLR4-dependent (Pfirschke et al., 2016). Moreover, $TLR4^+$ macrophages and DCs were shown to localize next to $HMGB1^+$ dying cells, suggesting that macrophages are activated upon recognition of DAMPs released from dying tumor cells (Stojanovska et al., 2018). Given the TLR signaling signature identified in macrophages early after Ox/Cy treatment, our data suggest that tumor macrophages are among the first immune cells activated by ICD. The influx of CAR-T cells after Ox/Cy further remodeled the TME, resulting in accumulation of M1 macrophages that provide the dominant source of chemokines mediating CAR-T cell recruitment into tumors. This population of $iNOS^+$ macrophages may arise from polarization of tumor-resident macrophages or from newly recruited cells.

Combination of CAR-T cell therapy with checkpoint blockade is being pursued in the clinic as a strategy to enhance CAR-T cell activity in solid tumors, and our data suggest that this strategy is only effective if a sufficient number of CAR-T cells penetrates and remodels tumors. Anti-PD-L1 treatment alone had no impact on CAR-T cell-mediated control of tumor growth. We only observed improvements in CAR-mediated tumor control when anti-PD-L1 was combined with Ox/Cy, which increased both numbers of $PD\text{-}1^+$ CAR-T cells and levels of PD-L1 on tumor macrophages. Moreover, although Ox/Cy and anti-PD-L1 blockade synergistically improved CAR-T cell mediated control of tumor growth in KP^{ROR1} mice, tumors in all mice eventually progressed despite repeated infusion Ox/Cy and CAR-T cells. Tumors from CAR-T cell treated mice retained expression of ROR1, indicating that antigen loss was not a mechanism of tumor escape in this model. Rather, CAR-T cells eventually became dysfunctional despite continued administration of anti PD-L1, suggesting that inhibitory pathways beyond the PD-1/PD-L1 axis need to be targeted to achieve durable tumor regression. Additional work is needed to understand the mechanisms that promote acquired CAR-T cell dysfunction (Lynn et al., 2019, Chen et al., 2019). Our data also reveal a heterogeneous response of individual tumors to Ox/Cy treatment, with larger tumors showing more limited upregulation of T cell-recruiting chemokines compared to smaller tumor. Progressive tumor growth is often associated with abnormal vascularization that results in hypoxia and limits efficient drug delivery (Azzi et al., 2013, Carmeliet and Jain, 2011), suggesting that inability of Ox/Cy to penetrate larger tumors may eventually drive tumor outgrowth. If drug accessibility is a reason for tumor outgrowth, strategies to normalize tumor vasculature to achieve more efficient drug delivery may be needed in combination (Carmeliet and Jain, 2011).

In summary, we developed a model for CAR-T cell therapy that is representative of a common human cancer, induced by oncogenic mutations, and has a TME populated by immunosuppressive cells. This model was superior at recapitulating the behavior of human ROR1 CAR-T cells in patients with $ROR1^+$ TNBC and NSCLC compared to transplantable models of the same diseases, mimicking their poor infiltration and acquired dysfunction in the TME. Achieving tumor regression in the KP model is notoriously difficult, and improved survival has not been previously demonstrated to our knowledge. Our data demonstrating a partial response in one TNBC patient treated with Ox/Cy and CAR-T cells provide a strong rationale for incorporating oxaliplatin into the lymphodepletion regimen to enhance ROR1 CAR-T infiltration into human lung and breast tumors and potentially improve efficacy.

Oxaliplatin is not typically combined with Cy or fludarabine, so this strategy may require evaluation of different dosing regimens to achieve sufficient lymphodepletion to promote CAR-T cell activity and preserve the TME-modifying effects of oxaliplatin. Nevertheless, this approach can be broadly applied in settings where engineered T cells are being investigated as a strategy to make “cold” tumors more permissive to adoptively transferred T cells.

STAR Methods

RESOURCE AVAILABILITY

Lead Contact—Further information and requests for resources and reagents should be directed to and will be fulfilled by the Lead Contact, Shivani Srivastava (ssrivas2@fhcrc.org).

Materials Availability—This study did not generate new unique reagents.

Data and Code Availability—The bulk and single-cell RNAseq expression datasets generated during this study have been deposited in the Gene Expression Omnibus under the accession number GSE158111.

EXPERIMENTAL MODEL AND SUBJECT DETAILS

Animals—C57BL/6 (B6), B6.SJL (CD45.1), BALB/cByJ, B6 *Cxcr3*$^{-/-}$, B6 *Cxcr6*$^{-/-}$, B6 *Ccr5*$^{-/-}$, and B6 *Ifng*$^{-/-}$ mice were purchased from Jackson Laboratory. *Kras*$^{LSL\text{-}G12D/+}$;*p53*$^{fl/fl}$ (KP) mice were generously provided by A. McGarry Houghton (FHCRC, Seattle WA). For studies with KP mice, 6–18 week old age-matched and sex-matched mice were used. For all other studies, 6–12 week old age-matched and sex-matched mice were used. Mice of the same sex were randomly assigned to experimental groups or were assigned based on tumor burden such that all experimental groups had similar average tumor volume prior to treatment. All mice were housed and bred at the FHCRC (Seattle, WA). All experiments were performed in accordance within the guidelines of the FHCRC Institutional Animal Care and Use Committee.

Human Subjects—The patients described in this report were enrolled on a phase 1 clinical trial evaluating autologous T cells engineered by lentiviral gene delivery to express a ROR1 CAR. The study is approved by the Institutional Review Board of the Fred Hutchinson Cancer Research Center and registered with ClinicalTrials.gov (NCT02706392), and informed consent was obtained from all subjects. The diagnosis and characteristics of the three patients treated on this trial and described in this report are provided in Table S1.

Cell Lines—The KP1233 (“KP”) tumor and 3TZ “GreenGo” cell lines were generously provided by Tyler Jacks (Massachusetts Institute of Technology). KP-ROR1 tumor cell lines were generated by retroviral transduction of the KP tumor cell line with full-length human *ROR1* cDNA (UniProt: Q01973) and subsequent FACS sorting of ROR1^{+} cells to >95% purity. 4T1 cell lines were purchased from the American Type Culture Collection and maintained in complete RPMI (RPMI 1640 with 10% FBS, 1 mM sodium pyruvate, 1 mM

HEPES, 100 U/ml penicillin/streptomycin, and 50 μM β-mercaptoethanol). MDA-MB-231 cells were purchased from ATCC and cultured in LCL media (RPMI 1640 with 5% FBS, 100 U/ml penicillin/streptomycin and 2 mM L-glutamine). Lenti-X cells for lentiviral packaging were purchased from Clontech. Plat-E cells for retroviral packaging were purchased from Cell Biolabs. All cells were tested bi-monthly for the absence of mycoplasma. KP, KP-ROR1, and 3TZ cell lines were maintained in complete DMEM (DMEM with 10% FBS, 2 mM L-glutamine, 100 U/ml penicillin/streptomycin, 25 mM HEPES).

METHOD DETAILS

Cloning of Murine CAR Constructs—The MP71 retroviral vector, which was a gift from W. Uckert (Max Delbruck Center for Molecular Medicine), was modified to encode either a human ROR1 (hROR1)-specific CAR or truncated murine CD19 (mp71-tCD19, UniProt: P25918, amino acids [aa] 1–321) for transduction of control murine T cells. For some experiments, the tCD19 transduction marker was fused to GFP (tCD19-GFP). The CAR possessed a murine CD8α signal peptide (UniProt: P01731, aa1–27), 2A2 scFv, human IgG4 short spacer (Hudecek et al., 2015), murine CD28 transmembrane (UniProt: P31041, aa151–177), murine 4–1BB (UniProt: P20334, aa211–256), murine CD3ζ (UniProt: P24161, aa52–164), and was linked by a P2A ribosomal skip element to murine truncated tCD19 or tCD19-GFP.

Generation of Murine CAR-T Cells—Retrovirus was produced by transient transfection (Clontech) of Plat-E cells with the indicated MP71 vectors. Viral supernatant was harvested 48 hr after transfection, filtered through a 0.45 μm pore filter, and snap-frozen in liquid nitrogen for long-term storage. Cell suspensions were prepared from spleen and peripheral lymph nodes of donor mice by tissue disruption with glass slides and filtered through a 40 μm filter. Murine $CD8^+$ and/or $CD4^+$ T cells were enriched from spleens and peripheral lymph nodes of donor mice using untouched negative isolation kits (Stem Cell) and stimulated with 1μg/ml each of plate-bound anti-CD3 and anti-CD28 (clone 145–2C11 and 37.51, respectively) for 24 hr in a 37°C, 5% CO_2 incubator in complete RPMI (RPM1 1640, 10% heat inactivated FBS, 1 mM sodium pyruvate, 1 mM HEPES, 100 U/ml penicillin/streptomycin, 50 μM β-mercaptoethanol) supplemented with 50 U/ml recombinant murine IL-2 (Peprotech). 24-well non-tissue culture plates were coated with 12.5 μg/ml RetroNectin (TaKaRa) according to the manufacturer's protocol, and plates were loaded with 1 ml pre-titered virus per well and centrifuged for 2 hr at 3000xg at 32°C. Murine T cells were harvested from anti-CD3/28-coated plates and resuspended to 1×10^6 cells/ml in complete RPMI supplemented with 50 U/ml IL-2 and anti-CD3/28 mouse T-activator Dynabeads (ThermoFisher) at a bead to cell ratio of 1:1. Viral supernatant was aspirated from RetroNectin-coated plates, plates were rinsed with PBS, and 1 ml (1×10^6) T cells were added to each virus-coated well. Plates were then centrifuged at 800g for 30 min at 32°C and returned to 37°C, 5% CO_2 incubators. After 24 hours, T cells were harvested and resuspended in complete RPMI with 50 U/ml IL-2. T cells were subsequently harvested, counted, and resuspended in complete RPMI with 50 ng/ml IL-15 every 1–2 days after. Four days after transduction, magnetic beads were removed and T cell transduction was measured by flow cytometry staining for tCD19, GFP and/or ROR1 CAR. Transduced cells were

enriched by positive selection using anti-CD19 microbeads (Miltenyi) and adoptively transferred into tumor-bearing KP mice.

Generation of Human ROR1 CAR-T Cells—Enrichment of $CD4^+$ and $CD8^+$ T cells was performed on aliquots of a leukapheresis or 400 mL blood draw obtained by venipuncture from each patient. Selection of $CD8^+$ and $CD4^+$ cells was performed identically using cGMP compliant CliniMACS® CD8 or CD4 Reagent systems (Miltenyi Biotec), following the manufacturers recommendations. Enriched $CD4^+$ and $CD8^+$ cells were stimulated in separate cultures in T-75 flasks with clinical grade anti-CD3 and anti-CD28 coated paramagnetic beads supplemented with CTL media (RPMI 1640 with 10% human serum, 2 mM L-glutamine, 25mM HEPES, penicillin/streptomycin (100U/ml), 50 μM β-mercaptoethanol) and 50 IU/mL IL-2. $CD4^+$ and $CD8^+$ cells were transduced with R12-ROR1 CAR lentiviral vector on day 1 after anti-CD3/CD28 bead stimulation. The lentivirus encoded a ROR1 CAR consisting of the R12 scFv, 4–1BB and CD3z signaling domains and a truncated epidermal growth factor receptor downstream of a T2A ribosomal skip site (Hudecek et al., 2013, Wang et al., 2011). Anti-CD3/CD28 beads were removed by magnetic depletion on day 3 – 5 post-stimulation. $CD4^+$ and $CD8^+$ cells were expanded in G-Rex flasks with CTL media + 50 IU/mL IL-2. Cells were harvested from each culture on day 12–16 after anti-CD3/CD28 stimulation, and a combined 1:1 CAR-transduced $CD4^+/CD8^+$ T cell product was formulated for cryopreservation and infusion. Patients were pretreated with cytoreductive chemotherapy and received the T cell infusion intravenously at least 48 hours after completing chemotherapy. Patients X475 and X461 were treated at dose level 1 (3.3×10^5 CART cells/kg) and X552 at dose level 2 (1×10^6 CART cells/kg). Each of these three patients exhibited high levels of CAR-T cell expansion in the blood that facilitated phenotypic and functional analysis.

CAR-T Cell Treatment of KP^{ROR1} mice—KP mice were scanned by MRI one week before T cell infusion and tumor volume was calculated for each mouse. Mice were distributed into treatment groups such that the average tumor volume and range in tumor volume in each group was as similar as possible prior to treatment to control for variability in induction of tumors. For all T cell infusion experiments, KP mice were pre-conditioned with intraperitoneal injection of 150 mg/kg cyclophosphamide and 5– 6 hr later were injected intravenously by retro-orbital or tail vein injection with 6×10^6 control or ROR1 CAR-T cells (1:1 ratio of CD8:CD4 T cells). Mice received cyclophosphamide and T cells every 3 weeks for the duration of the experiment where indicated. For co-transfer experiments, WT and *Cxcr3*$^{-/-}$, *Cxcr6*$^{-/-}$, or *Ccr5*$^{-/-}$ ROR1 CAR-T cells were mixed 1:1 prior to infusion. Mice were monitored for weight, body condition score, tumor burden, and survival where indicated. All mice in each experiment were sacrificed when any individual mice showed clinical signs of severe disease or 20 percent weight loss.

Ox/Cy and PD-L1 Treatment—Tumor-bearing KP mice were injected with 2.5 mg/kg Ox and 50 mg/kg Cy (Ox/Cy) or vehicle intraperitoneally once a week for three weeks. For experiments analyzing the effect of Ox/Cy on CAR-T anti-tumor activity and survival, this regimen was modified such that tumor-bearing KP^{ROR1} received intraperitoneal injections of Ox/Cy on day −14, day −7, and day 0 post T cell infusion. The third dose of Ox/Cy was

given 5–6 hr prior to T cell infusion and was modified to administer 2.5 mg/kg Ox with 150 mg/kg Cy to induce sufficient lymphodepletion prior to T cell infusion. Control mice received intraperitoneal injections of vehicle on day −14 and day −7 and on day 0 were treated with 150 mg/kg Cy 5–6 hr prior to T cell infusion to induce lymphodepletion. In some experiments, mice were treated with 200 ug anti-PD-L1 antibody intraperitoneally every 3–4 days beginning 1 day post T cell transfer. For experiments examining long-term anti-tumor efficacy and survival, KP^{ROR1} mice were infused with control or ROR1 CAR-T cells every 3 weeks and received 2.5 mg/kg Ox and 150 mg/kg Cy (Ox/Cy) or 150 mg/kg Cy alone as a control 5–6 hr prior to each T cell infusion.

CAR-T Cell Treatment of 4T1/hROR1 mice—BALB/cByJ female mice were impanted subcutaneously in the right 4^{th} mammary fat pad with 1×10^5 4T1 cells engineered to express human ROR1 (4T1-hROR1). After 14 days, mice were injected intraperitoneally with 150 mg/kg cyclophosphamide with or without 2.5 mg/kg oxaliplatin and 5–6 hr later were injected with 6×10^6 $CD8^+$ and $CD4^+$ (1:1 ratio) control or ROR1 CAR-T cells. Mice were treated with 200 ug anti-PD-L1 antibody intraperitoneally every 3–4 days beginning 1 day post T cell transfer. Tumor size was monitored using calipers, and tumor volume was calculated as (length in mm)*(width in mm)^2. Mice were sacrificed when any individual mouse showed clinical signs of severe disease or 20 percent weight loss.

Preparation of Tissues—A tumor biopsy was obtained by core needle biopsy from patient X475 The biopsy sample was disaggregated mechanically and tissue was mashed through a cell strainer with the plunger of a syringe. Single cell suspension was washed and prepared for flow cytometry analysis as indicated. For disaggregation of patient core needle biopsy, mechanical procedure using scalpels was applied and tissue was mashed through a cell strainer with the plunger of a syringe. Single cell suspension was washed and prepared for flow cytometry analysis as indicated. Tumor biopsies from patient X566 were fixed in 10% neutral-buffered formalin and used for IHC analysis.

Cell suspensions were prepared from murine spleen and peripheral lymph nodes by tissue disruption with glass slides, filtering through a 40 μm filter, and lysing with ACK lysis buffer (Gibco). For analysis of murine peripheral blood, blood was collected by retro-orbital bleeds into EDTA FACS tubes and underwent two rounds of lysis with ACK lysis buffer (Gibco). For bulk and single-cell RNAseq analysis of lung tumors and evaluation of WT vs. *Cxcr3*$^{-/-}$, *Cxcr6*$^{-/-}$, or *Ccr5*$^{-/-}$ ROR1 CAR-T tumor infiltration, individual tumor nodules were excised from lungs using a dissecting microscope. For all other experiments analyzing lung tumors, mice were injected with 10 ug PE-conjugated anti-CD45 antibody (clone 30-F11, BioLegend) intravenously via retro-orbital injection 5 min prior to euthanasia to distinguish vascular and non-vascular cells in the lung. Whole lungs were then collected and minced into 1–2 mm size fragments with scissors. Minced lungs or excised tumors were then digested into single cell suspensions using the Mouse Tumor Dissociation Kit (Miltenyi) for 1 hr at 37°C with gentle agitation. Cells were filtered through a 100 μm filter, lysed with ACK lysing buffer (Gibco), and resuspended as single cell suspensions for downstream analysis.

Flow Cytometry—For staining of murine cells, cells were stained using the Live/Dead Fixable Aqua Dead Cell stain kit (Invitrogen) according to the manufacturer's protocol. For surface staining, cells were incubated at 4°C for 30 min in staining buffer (PBS, 2% FBS) with the following directly conjugated antibodies for murine proteins (from BioLegend unless otherwise specified): anti-CD4 (RM4–5), -CD8 (53–6.7), -CD45.1 (A20), -CD3 (145–2C11), -CD19 (eBio1D3, Thermo Fisher), -CD45 (30-F11), -CD45.2 (104), -PD-1 (29F.1A12), -LAG-3 (C9B7W), -TIM3 (RMT3–23), -CXCR3 (CXCR3–173), -CXCR6 (SA051D1), -CCR5 (HM-CCR5), -CD25 (PC61.5, Thermo Fisher), -CD44 (IM7, Thermo Fisher), -TIGIT (IG9), -CD11b (M1/70), -CD11c (N418), -Ly6C (HK1.4, Thermo Fisher), -Ly6G (1A8), -F4/80 (BM8), I-A/I-E (M5/114.15.2, Thermo Fisher), -CD24 (M1/69), -CD64 (X54–5/7.1), -SiglecF (E50–2440, BD Biosciences), -PD-L1 (10F.9G2), -EpCAM (G8.8, Thermo Fisher); or with the following directly conjugated antibodies for human proteins: anti-ROR1 (2A2, Miltenyi Biotec). Recombinant Fc-hROR1 (Fred Hutchinson Cancer Research Center Protein Core) and anti-human IgG secondary antibody (HP6017, BioLegend) was used to measure ROR1 CAR expression. For intracellular staining, cells were surface stained as described, washed and permeabilized for 20 min with eBioscience Fix/Perm buffer at 4°C. Cells were stained for 30 min at 4°C in 1X Perm/Wash staining medium (eBioscience) with anti-mouse IFN-γ (XMG1; Thermo Fisher), -TNFα (MP6XT22, Thermo Fisher), -Foxp3 (FJK-16S), -Ki67 (B56, BD Biosciences), -CTLA-4 (UC10–4B9, Thermo Fisher), -CD206 (C068C2), and/or -iNOS (CXNFT, Thermo Fisher).

For intracellular cytokine staining following restimulation, digested lung single cell suspensions were stimulated with 50ng/ml PMA and 1 μg/ml ionomycin in 0.2 ml complete RPMI in 96-well U-bottomed plates (Costar) at 37°C, 5% CO_2 for 6 hr. GolgiPlug (BD Biosciences) was added to all wells according to the manufacturer's protocol at the beginning of co-culture. Data were acquired on LSRII, Canto 2 or Symphony flow cytometers (BD Biosciences) and analyzed using FlowJo software (Treestar).

The phenotype of R12-ROR1 CAR T cells in the infusion product and blood was determined by staining of cryopreserved patient samples. Freshly thawed patient samples were stained for 15 min at 4°C with fixable viability dye eFluor506 (Thermo Fisher), washed, and resuspended in staining buffer containing human Fc block (Miltenyi, 1:5). To detect human truncated EGFR (tEGFR) protein clinical grade monoclonal antibody (Erbitux) was biotinylated using EZ-Link Sulfo-NHS-Biotin (Thermo Fisher) and detected using conjugated streptavidin dye (BioLegend). Cells were incubated with biotinylated Erbitux mAb for 20 min at 4°C with and washed 2–3 times before adding antibody/streptavidin surface staining cocktail. For surface staining, cells were incubated at 4°C for 30 min in staining buffer (PBS, 2% FBS) with the following directly conjugated antibodies for human proteins (from BioLegend unless otherwise specified): anti-CD3 (UCHT1, BD Biosciences), CD4 (SK3, BD Biosciences), -CD8 (SK1, HIT8a, BD Biosciences), -CD45 (2D1, BD Biosciences), -PD-1 (EH12.2H7), -TIM-3 (F38–2E2, Thermo Fisher), -LAG-3 (3DS223H, Thermo Fisher), -TIGIT (MBSA43, Thermo Fisher), Mouse IgG1,k (BD Biosciences). After another wash step, cells were resuspended in BD Cytofix solution (1:4) and stored at 4°C in the dark until analysis.

qPCR—Individual lung tumors were excised using a dissecting microscope and immediately lysed in 1 ml buffer RLT (QIAGEN) using a gentleMACS Dissociator (Miltenyi). RNA was extracted using the RNeasy Mini kit (QIAGEN) and cDNA synthesized using the RT2 First Strand Kit (QIAGEN) with 500 ng RNA per sample. Expression of various chemokines was analyzed normalized to a housekeeping gene panel using the "Cancer Inflammation and Immunity Crosstalk" RT2 Profiler PCR Array (QIAGEN). Expression of *Cxcl16* was analyzed and normalized to *mActb*. Amplifications were performed for 50 cycles on an ABI Prism 7900 (Applied Biosystems) in a 20 μl reaction consisting of Power SYBR Green PCR Master Mix (Applied Biosystems), 5 ng of cDNA, and 500 nM gene-specific forward and reverse primers: *Cxcl16*, 5'-AAAGAGTGTGGAACTGGTCATG-3' and 5'-AGCTGGTGTGCTAGCTCCAG-3'(Rosito et al., 2012); *Actb*, 5'-CTGTCCCTGTATGCCTCTG-3' and 5'-ATGTCACGCACGATTTCC-3'. The cycle threshold (Ct) was determined using SDS software (Applied Biosystems) and the level of gene expression calculated using the comparative Ct method (2(^Ct)).

CBC Analysis—Peripheral blood was collected by retro-orbital bleeds into EDTA FACS tubes. Blood in EDTA FACS tubes was submitted to Phoenix Central Labs for complete blood count analysis with differential.

Luminex Assay—IFNγ, TNFα, and GM-CSF production by EGFRt positive T cells was measured by Luminex assay. $EGFRt^+$ $CD8^+$ and $CD4^+$ CAR T cells were FACS-purified from the infusion product and post treatment blood samples, and 50,000 T cells were seeded in 100 μl culture media (RPMI 1640, 10% human Serum, 4 mM L-Glutamine, 100 U/ml penicillin/streptomycin, 50 μM β-mercaptoethanol) in duplicate wells of non-tissue culture treated 96-well plates coated with 1 μg/ml anti-CD3 and anti-CD28 (clone OKT3 and CD28.2, BioLegend) monoclonal antibody. The plates were incubated at 37 °C for 3 days. Following the incubation, supernatants were harvested and Luminex assays were performed. xPONENT software was used for curve fitting and data analysis.

Tumor Assessment, Toxicity Grading, and Outcome—Anti-tumor activity of R12-ROR1 CAR T cells was assessed by RECIST (1.1). The response categories were as follows: Progressive Disease (PD), at least a 20% increase in the sum of diameters of target lesions or appearance of new lesions, taking as reference the smallest sum on study (this includes the baseline sum if that is the smallest on study), and an absolute increase in the sum of diameters of at least 5 mm; Partial Response (PR): at least a 30% decrease in the sum of diameters of target lesions, taking as reference the baseline sum diameters; Stable Disease (SD): neither sufficient shrinkage to qualify for PR nor sufficient increase to qualify for PD, taking as reference the smallest sum diameters while on study. Dose-limiting toxicity (DLT) evaluation period was 28 days following CAR T cell infusion.

Generation, Titration, and Intratracheal Administration of Cre Lentivirus—To generate Cre-expressing lentivirus, we modified the HIV7 lentiviral vector (Yam et al., 2002) to encode Cre recombinase linked by a P2A ribosomal skip element to firefly luciferase (Cre-ffluc lentivirus). To generate Cre and ROR1-expressing lentivirus, the HIV7

vector was modified to encode Cre recombinase linked by a P2A ribosomal skip element to firefly luciferase, which was linked by a T2A ribosomal skip element to human truncated ROR1 (UniProt: Q01973, aa 1–462) (Cre-ffluc-hROR1 lentivirus).

Lentivirus was produced by transient calcium phosphate transfection of the packaging cell line LentiX with the indicated HIV7 lentiviral vectors, psPAX2 (Addgene #12260), and VSVg envelope. Viral supernatant was harvested 24, 48 and 72 hr after transfection, filtered through a 0.45-μm pore filter, and stored at 4°C for up to 1 week until ready for ultracentrifugation. Lentivirus was concentrated by mixing filtered lentivirus with 40% polyethylene glycol (PEG, Sigma) at a PEG to virus ratio of 1:3 for 12–24 hr at 4°C. The virus/PEG mixture was then centrifuged at 1500g for 45 min at 4°C, supernatant was aspirated, and the virus pellet was resuspended in 30 ml serum-free DMEM. Lentivirus was further concentrated in an Optima L-90K ultracentrifuge (Beckman Coulter) at 24,500 rpm for 90 min at 4°C. The final virus pellet was resuspended in 0.5 – 1 ml serum-free DMEM by vortexing for 1–3 hr at 4°C, aliquoted, and frozen at −80°C for long-term storage.

Cre lentivirus was titered using 3TZ “Green Go” cells. Briefly, 5×10^4 3TZ cells were plated in 1 ml of complete DMEM in 12-well plates. 5–6 hours later when cells were adherent, supernatant was aspirated and media was replaced with 0.5 ml complete DMEM containing serial dilutions of thawed Cre lentivirus (e.g. 10-fold serial dilutions from 1:10 to 1:10,000) and 8 μg/ml polybrene. After 24 hr, media was replaced with 1 ml complete DMEM and cells were passaged for 3–4 days before analysis by flow cytometry for GFP and/or ROR1 expression. Virus titer was calculated according to the following formula: Titer (pfu/μl) = [(5×10^4) * (%GFP^+ cells) / 100] / [Volume of virus added (μl)]. Lung tumors were induced in KP mice by intratracheal intubation and inhalation of 1×10^4 – 1×10^5 pfu Cre-expressing lentivirus as reported.

Metastatic Transplantable KP Tumor Model—5×10^4 KP or KP-ROR1 tumor cell lines were injected intravenously via tail vein into 6–8 week old B6 mice. After 28 days, mice were injected intraperitoneally with 150 mg/kg cyclophosphamide and 5–6 hr later injected with 6×10^6 control or ROR1 CAR-T cells (1:1 ratio of CD8:CD4 T cells).

Bioluminescent Imaging—For bioluminescence imaging of tumors *in vivo*, mice received intraperitoneal injections of luciferin substrate (Caliper Life Sciences) resuspended in PBS (15 μg/g body weight). Mice were anesthetized with isoflurane and imaged using an Xenogen IVIS Imaging System (Caliper). For imaging of cell lines, ~1×10^5 cells were plated in 6-well plates. After 24–48 hr when cells were adherent, supernatant was aspirated and replaced with complete DMEM supplemented with 150ug/ml luciferin substrate. Images were acquired at 10, 12 and 14 min after luciferin injection of mice, and after 2, 4, and 6 min after luciferin addition to cells, in small binning mode at an acquisition time of 1 s to 1 min to obtain unsaturated images. Luciferase activity was analyzed using Living Image Software (Caliper) and the photon flux analyzed within regions of interest that encompassed the entire body of each individual mouse or the entire cell culture well.

Magnetic Resonance Imaging and Analysis of Tumor Burden—Mice were imaged on a 1-Tesla Bruker ICON™ MRI scanner. Animals were anesthetized with 1–3% isoflurane

via induction chamber, then maintained on a nose cone. A gradient echo flow compensated sequence using a repetition time of 592.4 ms, echo time of 7.0 ms and flip angle of 80° were used throughout the study. The slice thickness was 1 mm, and the number of slices was 15, which was sufficient to cover the entire lung. The acquisition matrix size was 128 × 178, the reconstructed matrix size was 128 × 256, and the field of view was 25 × 25 mm^2. Motion artifacts were minimized by application of respiratory gating to all MRI studies. All animals were scanned by using the described settings and parameters. Tumor burden was analyzed using ImageJ or Vivoquant software (Invicro). Briefly, region of interest (ROI) tools were used to annotate individual lung tumor nodules in each mouse at each time point. Volume of each tumor nodule was calculated by multiplying the tumor area (mm^2) by the slice thickness (1 mm). Percent change in tumor volume was calculated using the following formula: [(Vol. at $Time_X$) – (Vol. at $Time_0$)] / [Vol. at $Time_0$] * 100, where $Time_0$ is one week prior to CAR-T cell treatment.

Immunohistochemistry—Formalin-fixed paraffin-embedded tissues were sectioned at 4 microns onto positively-charged slides and baked for 1 hr at 60°C. The slides were then dewaxed and stained on a Leica BOND Rx autostainer (Leica, Buffalo Grove, IL) using Leica Bond reagents for dewaxing (Dewax Solution). Antigen retrieval was performed at 100°C for 20 min using Leica Epitope Retrieval Solution 2. Endogenous peroxidase was blocked with 3% H_2O_2 for 5 min followed by protein blocking with TCT buffer (0.05 M Tris, 0.15 M NaCl, 0.25% Casein, 0.1% Tween 20, pH 7.6 +/− 0.1) for 10 min. Primary rat anti-CD3 antibody at 1:250 (Serotec #MCA1477) or primary rabbit anti-ROR1 antibody at 1:25 (Cell Signaling #4102) was applied for 60 minutes followed by the secondary rabbit anti-rat antibody at 1:500 (Rockland #712–4126) for 20 min. Staining was visualized using Dako Envision Plus, HRP Rabbit specific polymer, for 12 min followed by 3,3'-diaminobenzidine (DAB, Dako) for 10 min. The sections were counter-stained with Dako hematoxylin for 3 min and then cover-slipped. Concentration matched isotype control slides were performed for each antibody on each tissue sample. Percent $CD3^+$ cells within tumors were quantified using HALO software (Indica Labs). Scoring of $CD3^+$ localization within tumors were performed in a blinded fashion by a veterinary pathologist.

For multiplex IHC staining of patient needle biopsies, formalin-fixed paraffin-embedded tissues were stained on a Leica BOND Rx autostainer using the Akoya Opal Multiplex IHC assay (Akoya Biosciences, Menlo Park, CA) with the following changes: Additional high stringency washes were performed after the secondary antibody and Opal fluor applications using high-salt TBST (0.05M Tris, 0.3M NaCl, and 0.1% Tween-20, pH 7.2–7.6). TCT was used as the blocking buffer (0.05M Tris, 0.15M NaCl, 0.25% Casein, 0.1% Tween 20, pH 7.6 +/− 0.1). Samples were stained with the following primary antibodies incubated for 1 hour at room temperature; anti-CD3 (Thermo), -COX2 (BSB), -CD206 (Novus), -VISTA (Cell Signaling), -B7H3 (BSB), -CD163 (BioSB). OPAL Polymer HRP Mouse plus Rabbit (Akoya Biosciences, Menlo Park, CA) was used for all secondary applications. Slides were mounted with ProLong Gold and cured for 24 hours at room temperature in the dark before image acquisition at 20x magnification on the Akoya Vectra 3.0 Automated Imaging System. Vectra images were spectrally unmixed using Akoya Phenoptics inForm software. Cellular analysis of the images was performed using HALO image analysis software (Indica

Labs, Corrales, NM). Mean fluorescence intensity of the nucleated (DAPI+) cells was used to determine positivity for each marker. The positive cell data was then used to define percentage and density of positive cells in the tumor and stroma regions of interest (ROI).

Bulk RNAseq—Individual lung tumors were excised using a dissecting microscope and immediately lysed in 1 ml buffer RLT (QIAGEN) using a gentleMACS Dissociator (Miltenyi). RNA was extracted using the RNeasy Mini kit (QIAGEN) according to the manufactuer's instructions. Total RNA integrity was checked using an Agilent 4200 TapeStation (Agilent Technologies) and quantified using a Trinean DropSense96 spectrophotometer (Caliper Life Sciences). RNA-seq libraries were prepared from total RNA using the TruSeq RNA Sample Prep Kit v2 (Illumina) and a Sciclone NGSx Workstation (PerkinElmer). Library size distributions were validated using an Agilent 4200 TapeStation. Additional library quality control, blending of pooled indexed libraries, and cluster optimization were performed using a Qubit 2.0 Fluorometer (Thermo Fisher Scientific). RNA-seq libraries were pooled (6- to 8-plex) and clustered onto a flow cell lane. Sequencing was performed using an Illumina HiSeq 2500 in rapid mode using a paired-end, 50-base read length sequencing strategy.

We used STAR(Sinden et al., 1990) to align reads to a custom reference genome which included a standard mouse genome (University of California, Santa Cruz Mouse Genome Assembly GRCm38 reference) in addition to the genome of the lentivirus and retrovirus used for tumor induction and CAR-T manufacturing, respectively. Gene quantification from trimmed reads was performed using the Bioconductor Package, GenomicAlignments. (Lawrence et al., 2013) Genes with less than 10 total nonzero read counts across the entire data set were discarded as were genes that were not annotated with a human gene symbol. This resulted in 15,191 genes used in downstream differential expression and enrichment analysis. The DESeq2 package (Love et al., 2014) was used to calculate differential expression and to perform a shrinkage of log2 fold change values. A log2 fold change threshold of 1 and an FDR threshold of 1% were used to determine differentially expressed genes. Gene Set Enrichment Analysis was performed using the piano package (Varemo et al., 2013) with enrichment terms taken from the Molecular Signatures Database v6.2 (Subramanian et al., 2005).

Single-cell RNA sequencing—Tumors were excised and pooled from individual KP^{ROR1} mice using a dissecting microscope (5–15 tumors per mouse), processed as described above, and cryopreserved in FBS + 10% DMSO. $CD8^{+}$ ROR1 CAR-T cells from infusion products were likewise cryopreserved in FBS + 10% DMSO. Samples were subsequently thawed, washed, and labeled in a single cell fashion using the 10X Genomics 3' Chromium v2.0 platform as per the manufacturer's instructions. Libraries were generated per the manufacturer's protocol and were sequenced on an Illumina HiSeq 2500 "rapid run" mode according to the standard 10X Genomics protocol. Resulting reads were aligned to the custom reference genome as described above using Cellranger software (10X Genomics) and "aggregated" to downsample all reads to equivalent levels across samples. Cells whose UMI counts for mitochondrial genes greater than 10% were excluded from downstream analysis. Cells with between 200 and 20000 genes expressed per cell were included in the

analysis. Scrublet (Wolock et al., 2019) was used to identify potential multiplets which were excluded from downstream analysis. We targeted 10,000 cells for capture and obtained the following total numbers of cells for each sample after filtering cells for quality: 3068 (D0 untreated), 3791 (D0 Ox/Cy), 2587 (D10 Cy + CAR-T cells), 4140 (D10 OxCy + CAR-T cells), 3086 (CAR infusion product).

Clustering, Differential Expression, GSEA and Geneset Scores—All clustering was performed using Monocle3 (Cao et al., 2019). For unsupervised clustering of cell expression profiles, expression matrices from Cellranger were first normalized by size factors. Dimensionality reduction using PCA/UMAP, in addition to differential expression was calculated using Monocle3. GSEA on single cell data expression data was performed by first ranking gene expression between two groups of cells using the full model coefficient derived from the differential expression function in Monocle3. Secondly, these ranked lists were interrogated for enrichment (using the Piano package) for any given geneset. Single cell geneset scores were calculated by taking the sum of the normalized pseudocount for all genes in the geneset.

Neural network annotation—To identify congruency with previously published single cell expression profiles of murine lung tumors (GSE127465 (Zilionis et al., 2019)), we first identified those features common to both our data and the GSE127465 data using mouse gene symbols (16,460). We then performed Term Frequency, Inverse Document Frequency normalization as previously described (Cusanovich et al., 2018) on both datasets, in an effort to highlight cell-specific features and to scale expression values from 0 to 1. Using an R implementation of the keras API, we trained a neural network on 20% of the cells in GSE127465. On the remaining 80% the model achieved a 94.1% accuracy. The neural network was comprised of two dense layers: the first layer had units of cell number * 0.1 and used a rectified linear unit activation function; the second layer had 24 units and used softmax activation. The model was compiled with a RMSprop optimizer and used categorical crossentropy as a loss function.

QUANTIFICATION AND STATISTICAL ANALYSIS

All data are presented as the mean values ± SEM. Statistical significance was determined by one-way ANOVA with Tukey's post-test, two-way ANOVA with Tukey's post-test, log-rank Mantel-Cox test, unpaired Student's two-way t-test, or paired Student's two-way t-test as indicated in figure legends using Prism software (Graphpad). Statistical significance was established at the levels of *, $p<0.05$; **, $p<0.005$; ***, $p<0.0005$; ****, $p<0.0001$.

ADDITIONAL RESOURCES

The ROR1 CAR-T cell clinical trial is registered with ClinicalTrials.gov (NCT02706392).

Supplementary Material

Refer to Web version on PubMed Central for supplementary material.

Acknowledgements

This work was supported by grants from the National Institutes of Health (R01CA114536; P50CA22894), Cancer Center Support Grant (P30 CA015704), and Juno Therapeutics, a Celgene Company. S.S. is a Cancer Research Institute Irvington Fellow supported by the Cancer Research Institute. We wish to thank Joshua Veatch, Mark Headley, Tyler Jacks, and Wolfgang Uckert for helpful discussions and reagents. Treatment schematic figures and graphical abstract were created with BioRender.

References

ADUSUMILLI PS, CHERKASSKY L, VILLENA-VARGAS J, COLOVOS C, SERVAIS E, PLOTKIN J, JONES DR & SADELAIN M 2014 Regional delivery of mesothelin-targeted CAR T cell therapy generates potent and long-lasting CD4-dependent tumor immunity. Sci Transl Med, 6, 261ra151.

ANDERSON KG, MAYER-BARBER K, SUNG H, BEURA L, JAMES BR, TAYLOR JJ, QUNAJ L, GRIFFITH TS, VEZYS V, BARBER DL & MASOPUST D 2014 Intravascular staining for discrimination of vascular and tissue leukocytes. Nat Protoc, 9, 209–22. [PubMed: 24385150]

AZZI S, HEBDA JK & GAVARD J 2013 Vascular permeability and drug delivery in cancers. Front Oncol, 3, 211. [PubMed: 23967403]

BALAKRISHNAN A, GOODPASTER T, RANDOLPH-HABECKER J, HOFFSTROM BG, JALIKIS FG, KOCH LK, BERGER C, KOSASIH PL, RAJAN A, SOMMERMEYER D, PORTER PL & RIDDELL SR 2017 Analysis of ROR1 Protein Expression in Human Cancer and Normal Tissues. Clinical cancer research : an official journal of the American Association for Cancer Research, 23, 3061–3071. [PubMed: 27852699]

BERGER C, SOMMERMEYER D, HUDECEK M, BERGER M, BALAKRISHNAN A, PASZKIEWICZ PJ, KOSASIH PL, RADER C & RIDDELL SR 2015 Safety of targeting ROR1 in primates with chimeric antigen receptor-modified T cells. Cancer immunology research, 3, 206–216. [PubMed: 25355068]

BROWN CE, ALIZADEH D, STARR R, WENG L, WAGNER JR, NARANJO A, OSTBERG JR, BLANCHARD MS, KILPATRICK J, SIMPSON J, KURIEN A, PRICEMAN SJ, WANG X, HARSHBARGER TL, D'APUZZO M, RESSLER JA, JENSEN MC, BARISH ME, CHEN M, PORTNOW J, FORMAN SJ & BADIE B 2016 Regression of Glioblastoma after Chimeric Antigen Receptor T-Cell Therapy. N Engl J Med, 375, 2561–9. [PubMed: 28029927]

BROWN CE, BADIE B, BARISH ME, WENG L, OSTBERG JR, CHANG W-C, NARANJO A, STARR R, WAGNER J, WRIGHT C, ZHAI Y, BADING JR, RESSLER JA, PORTNOW J, D'APUZZO M, FORMAN SJ & JENSEN MC 2015 Bioactivity and Safety of IL13Rα2-Redirected Chimeric Antigen Receptor CD8+ T Cells in Patients with Recurrent Glioblastoma. Clinical cancer research : an official journal of the American Association for Cancer Research, 21, 4062–4072. [PubMed: 26059190]

CAO J, SPIELMANN M, QIU X, HUANG X, IBRAHIM DM, HILL AJ, ZHANG F, MUNDLOS S, CHRISTIANSEN L, STEEMERS FJ, TRAPNELL C & SHENDURE J 2019 The single-cell transcriptional landscape of mammalian organogenesis. Nature, 566, 496–502. [PubMed: 30787437]

CARMELIET P & JAIN RK 2011 Principles and mechanisms of vessel normalization for cancer and other angiogenic diseases. Nat Rev Drug Discov, 10, 417–27. [PubMed: 21629292]

CHEN J, LÓPEZ-MOYADO IF, SEO H, LIO C-WJ, HEMPLEMAN LJ, SEKIYA T, YOSHIMURA A, SCOTT-BROWNE JP & RAO A 2019 NR4A transcription factors limit CAR T cell function in solid tumours. Nature, 567, 530–534. [PubMed: 30814732]

CRADDOCK JA, LU A, BEAR A, PULE M, BRENNER MK, ROONEY CM & FOSTER AE 2010 Enhanced Tumor Trafficking of GD2 Chimeric Antigen Receptor T Cells by Expression of the Chemokine Receptor CCR2b. Journal of Immunotherapy, 33, 780–788. [PubMed: 20842059]

CUSANOVICH DA, REDDINGTON JP, GARFIELD DA, DAZA RM, AGHAMIRZAIE D, MARCO-FERRERES R, PLINER HA, CHRISTIANSEN L, QIU X, STEEMERS FJ, TRAPNELL C, SHENDURE J & FURLONG EEM 2018 The cis-regulatory dynamics of embryonic development at single-cell resolution. Nature, 555, 538–542. [PubMed: 29539636]

DANGAJ D, BRUAND M, GRIMM AJ, RONET C, BARRAS D, DUTTAGUPTA PA, LANITIS E, DURAISWAMY J, TANYI JL, BENENCIA F, CONEJO-GARCIA J, RAMAY HR, MONTONE KT, POWELL DJ JR., GIMOTTY PA, FACCIABENE A, JACKSON DG, WEBER JS, RODIG SJ, HODI SF, KANDALAFT LE, IRVING M, ZHANG L, FOUKAS P, RUSAKIEWICZ S, DELORENZI M & COUKOS G 2019 Cooperation between Constitutive and Inducible Chemokines Enables T Cell Engraftment and Immune Attack in Solid Tumors. Cancer Cell, 35, 885–900 e10. [PubMed: 31185212]

DUPAGE M, CHEUNG AF, MAZUMDAR C, WINSLOW MM, BRONSON R, SCHMIDT LM, CROWLEY D, CHEN J & JACKS T 2011 Endogenous T cell responses to antigens expressed in lung adenocarcinomas delay malignant tumor progression. Cancer cell, 19, 72–85. [PubMed: 21251614]

DUPAGE M, DOOLEY AL & JACKS T 2009 Conditional mouse lung cancer models using adenoviral or lentiviral delivery of Cre recombinase. Nature protocols, 4, 1064–1072. [PubMed: 19561589]

DUPAGE M & JACKS T 2013 Genetically engineered mouse models of cancer reveal new insights about the antitumor immune response. Current opinion in immunology, 25, 192–199. [PubMed: 23465466]

GARBE AI, VERMEER B, GAMREKELASHVILI J, WASIELEWSKI RV, GRETEN FR, WESTENDORF AM, BUER J, SCHMID RM, MANNS MP, KORANGY F & GRETEN TF 2006 Genetically induced pancreatic adenocarcinoma is highly immunogenic and causes spontaneous tumor-specific immune responses. Cancer research, 66, 508–516. [PubMed: 16397267]

GUEDAN S, RUELLA M & JUNE CH 2019 Emerging Cellular Therapies for Cancer. Annu Rev Immunol, 37, 145–171. [PubMed: 30526160]

GUO F, WANG Y, LIU J, MOK SC, XUE F & ZHANG W 2016 CXCL12/CXCR4: a symbiotic bridge linking cancer cells and their stromal neighbors in oncogenic communication networks. Oncogene, 35, 816–26. [PubMed: 25961926]

HARLIN H, MENG Y, PETERSON AC, ZHA Y, TRETIAKOVA M, SLINGLUFF C, MCKEE M & GAJEWSKI TF 2009 Chemokine Expression in Melanoma Metastases Associated with CD8+ T-Cell Recruitment. Cancer Research, 69, 3077–3085. [PubMed: 19293190]

HUDECEK M, LUPO-STANGHELLINI M-T, KOSASIH PL, SOMMERMEYER D, JENSEN MC, RADER C & RIDDELL SR 2013 Receptor affinity and extracellular domain modifications affect tumor recognition by ROR1-specific chimeric antigen receptor T cells. Clinical cancer research : an official journal of the American Association for Cancer Research, 19, 3153–3164. [PubMed: 23620405]

HUDECEK M, SCHMITT TM, BASKAR S, LUPO-STANGHELLINI M-T, NISHIDA T, YAMAMOTO TN, BLEAKLEY M, TURTLE CJ, CHANG W-C, GREISMAN HA, WOOD B, MALONEY DG, JENSEN MC, RADER C & RIDDELL SR 2010 The B-cell tumor-associated antigen ROR1 can be targeted with T cells modified to express a ROR1-specific chimeric antigen receptor. Blood, 116, 4532–4541. [PubMed: 20702778]

HUDECEK M, SOMMERMEYER D, KOSASIH PL, SILVA-BENEDICT A, LIU L, RADER C, JENSEN MC & RIDDELL SR 2015 The nonsignaling extracellular spacer domain of chimeric antigen receptors is decisive for in vivo antitumor activity. Cancer immunology research, 3, 125–135. [PubMed: 25212991]

JIANG P, GU S, PAN D, FU J, SAHU A, HU X, LI Z, TRAUGH N, BU X, LI B, LIU J, FREEMAN GJ, BROWN MA, WUCHERPFENNIG KW & LIU XS 2018 Signatures of T cell dysfunction and exclusion predict cancer immunotherapy response. Nat Med, 24, 1550–1558. [PubMed: 30127393]

JIN L, TAO H, KARACHI A, LONG Y, HOU AY, NA M, DYSON KA, GRIPPIN AJ, DELEYROLLE LP, ZHANG W, RAJON DA, WANG QJ, YANG JC, KRESAK JL, SAYOUR EJ, RAHMAN M, BOVA FJ, LIN Z, MITCHELL DA & HUANG J 2019 CXCR1- or CXCR2-modified CAR T cells co-opt IL-8 for maximal antitumor efficacy in solid tumors. Nat Commun, 10, 4016. [PubMed: 31488817]

KOCHENDERFER JN & ROSENBERG SA 2013 Treating B-cell cancer with T cells expressing anti-CD19 chimeric antigen receptors. Nature reviews. Clinical oncology, 10, 267–276.

KRYSKO DV, GARG AD, KACZMAREK A, KRYSKO O, AGOSTINIS P & VANDENABEELE P 2012 Immunogenic cell death and DAMPs in cancer therapy. Nat Rev Cancer, 12, 860–75. [PubMed: 23151605]

LANITIS E, DANGAJ D, IRVING M & COUKOS G 2017 Mechanisms regulating T-cell infiltration and activity in solid tumors. Ann Oncol, 28, xii18–xii32. [PubMed: 29045511]

LAWRENCE M, HUBER W, PAGES H, ABOYOUN P, CARLSON M, GENTLEMAN R, MORGAN MT & CAREY VJ 2013 Software for computing and annotating genomic ranges. PLoS Comput Biol, 9, e1003118. [PubMed: 23950696]

LI J, BYRNE KT, YAN F, YAMAZOE T, CHEN Z, BASLAN T, RICHMAN LP, LIN JH, SUN YH, RECH AJ, BALLI D, HAY CA, SELA Y, MERRELL AJ, LIUDAHL SM, GORDON N, NORGARD RJ, YUAN S, YU S, CHAO T, YE S, EISINGER-MATHASON TSK, FARYABI RB, TOBIAS JW, LOWE SW, COUSSENS LM, WHERRY EJ, VONDERHEIDE RH & STANGER BZ 2018 Tumor Cell-Intrinsic Factors Underlie Heterogeneity of Immune Cell Infiltration and Response to Immunotherapy. Immunity, 49, 178–193 e7. [PubMed: 29958801]

LIU G, RUI W, ZHENG H, HUANG D, YU F, ZHANG Y, DONG J, ZHAO X & LIN X 2020 CXCR2-modified CAR-T cells have enhanced trafficking ability that improves treatment of hepatocellular carcinoma. Eur J Immunol.

LOVE MI, HUBER W & ANDERS S 2014 Moderated estimation of fold change and dispersion for RNA-seq data with DESeq2. Genome Biol, 15, 550. [PubMed: 25516281]

LYNN RC, WEBER EW, SOTILLO E, GENNERT D, XU P, GOOD Z, ANBUNATHAN H, LATTIN J, JONES R, TIEU V, NAGARAJA S, GRANJA J, BOURCY CFAD, MAJZNER R, SATPATHY AT, QUAKE SR, MONJE M, CHANG HY & MACKALL CL 2019 c-Jun overexpression in CAR T cells induces exhaustion resistance. Nature, 576, 293–300. [PubMed: 31802004]

MACMICKING J, XIE QW & NATHAN C 1997 Nitric oxide and macrophage function. Annu Rev Immunol, 15, 323–50. [PubMed: 9143691]

MANTOVANI A, SOZZANI S, LOCATI M, ALLAVENA P & SICA A 2002 Macrophage polarization: tumor-associated macrophages as a paradigm for polarized M2 mononuclear phagocytes. Trends Immunol, 23, 549–55. [PubMed: 12401408]

MOON EK, CARPENITO C, SUN J, WANG L-CS, KAPOOR V, PREDINA J, POWELL DJ, RILEY JL, JUNE CH & ALBELDA SM 2011 Expression of a functional CCR2 receptor enhances tumor localization and tumor eradication by retargeted human T cells expressing a mesothelin-specific chimeric antibody receptor. Clinical cancer research : an official journal of the American Association for Cancer Research, 17, 4719–4730. [PubMed: 21610146]

NISHIO N & DOTTI G 2015 Oncolytic virus expressing RANTES and IL-15 enhances function of CAR-modified T cells in solid tumors. Oncoimmunology, 4, e988098. [PubMed: 25949885]

PENG W, YE Y, RABINOVICH BA, LIU C, LOU Y, ZHANG M, WHITTINGTON M, YANG Y, OVERWIJK WW, LIZÉE G & HWU P 2010 Transduction of tumor-specific T cells with CXCR2 chemokine receptor improves migration to tumor and antitumor immune responses. Clinical cancer research : an official journal of the American Association for Cancer Research, 16, 5458–5468. [PubMed: 20889916]

PEREIRA JP, AN J, XU Y, HUANG Y & CYSTER JG 2009 Cannabinoid receptor 2 mediates the retention of immature B cells in bone marrow sinusoids. Nat Immunol, 10, 403–11. [PubMed: 19252491]

PFIRSCHKE C, ENGBLOM C, RICKELT S, CORTEZ-RETAMOZO V, GARRIS C, PUCCI F, YAMAZAKI T, POIRIER-COLAME V, NEWTON A, REDOUANE Y, LIN Y-J, WOJTKIEWICZ G, IWAMOTO Y, MINO-KENUDSON M, HUYNH TG, HYNES RO, FREEMAN GJ, KROEMER G, ZITVOGEL L, WEISSLEDER R & PITTET MJ 2016 Immunogenic Chemotherapy Sensitizes Tumors to Checkpoint Blockade Therapy. Immunity, 44, 343–354. [PubMed: 26872698]

PRICEMAN SJ, TILAKAWARDANE D, JEANG B, AGUILAR B, MURAD JP, PARK AK, CHANG WC, OSTBERG JR, NEMAN J, JANDIAL R, PORTNOW J, FORMAN SJ & BROWN CE 2018 Regional Delivery of Chimeric Antigen Receptor-Engineered T Cells Effectively Targets HER2(+) Breast Cancer Metastasis to the Brain. Clin Cancer Res, 24, 95–105. [PubMed: 29061641]

RIBAS A, DUMMER R, PUZANOV I, VANDERWALDE A, ANDTBACKA RHI, MICHIELIN O, OLSZANSKI AJ, MALVEHY J, CEBON J, FERNANDEZ E, KIRKWOOD JM, GAJEWSKI TF, CHEN L, GORSKI KS, ANDERSON AA, DIEDE SJ, LASSMAN ME, GANSERT J, HODI FS & LONG GV 2017 Oncolytic Virotherapy Promotes Intratumoral T Cell Infiltration and Improves Anti-PD-1 Immunotherapy. Cell, 170, 1109–1119 e10. [PubMed: 28886381]

ROSENBERG SA & RESTIFO NP 2015 Adoptive cell transfer as personalized immunotherapy for human cancer. Science (New York, N.Y.), 348, 62–68.

ROSITO M, DEFLORIO C, LIMATOLA C & TRETTEL F 2012 CXCL16 orchestrates adenosine A3 receptor and MCP-1/CCL2 activity to protect neurons from excitotoxic cell death in the CNS. J Neurosci, 32, 3154–63. [PubMed: 22378888]

RUD AK, BOYE K, ØIJORDSBAKKEN M, LUND-IVERSEN M, HALVORSEN AR, SOLBERG SK, BERGE G, HELLAND Å, BRUSTUGUN OT & MÆLANDSMO GM 2013 Osteopontin is a prognostic biomarker in non-small cell lung cancer. BMC Cancer, 13, 540. [PubMed: 24215488]

SANCHEZ-RIVERA FJ, PAPAGIANNAKOPOULOS T, ROMERO R, TAMMELA T, BAUER MR, BHUTKAR A, JOSHI NS, SUBBARAJ L, BRONSON RT, XUE W & JACKS T 2014 Rapid modelling of cooperating genetic events in cancer through somatic genome editing. Nature, 516, 428–31. [PubMed: 25337879]

SINDEN JD, ALLEN YS, RAWLINS JN & GRAY JA 1990 The effects of ibotenic acid lesions of the nucleus basalis and cholinergic-rich neural transplants on win-stay/lose-shift and win-shift/lose-stay performance in the rat. Behav Brain Res, 36, 229–49. [PubMed: 2310488]

SRIVASTAVA S & RIDDELL SR 2018 Chimeric Antigen Receptor T Cell Therapy: Challenges to Bench-to-Bedside Efficacy. Journal of immunology (Baltimore, Md. : 1950), 200, 459–468.

SRIVASTAVA S, SALTER AI, LIGGITT D, YECHAN-GUNJA S, SARVOTHAMA M, COOPER K, SMYTHE KS, DUDAKOV JA, PIERCE RH, RADER C & RIDDELL SR 2019 Logic-Gated ROR1 Chimeric Antigen Receptor Expression Rescues T Cell-Mediated Toxicity to Normal Tissues and Enables Selective Tumor Targeting. Cancer cell, 35, 489–503.e8. [PubMed: 30889382]

STASI AD, ANGELIS BD, ROONEY CM, ZHANG L, MAHENDRAVADA A, FOSTER AE, HESLOP HE, BRENNER MK, DOTTI G & SAVOLDO B 2009 T lymphocytes coexpressing CCR4 and a chimeric antigen receptor targeting CD30 have improved homing and antitumor activity in a Hodgkin tumor model. Blood, 113, 6392–6402. [PubMed: 19377047]

STOJANOVSKA V, MCQUADE RM, FRASER S, PRAKASH M, GONDALIA S, STAVELY R, PALOMBO E, APOSTOLOPOULOS V, SAKKAL S & NURGALI K 2018 Oxaliplatin-induced changes in microbiota, TLR4+ cells and enhanced HMGB1 expression in the murine colon. PLoS One, 13, e0198359. [PubMed: 29894476]

SUBRAMANIAN A, TAMAYO P, MOOTHA VK, MUKHERJEE S, EBERT BL, GILLETTE MA, PAULOVICH A, POMEROY SL, GOLUB TR, LANDER ES & MESIROV JP 2005 Gene set enrichment analysis: a knowledge-based approach for interpreting genome-wide expression profiles. Proc Natl Acad Sci U S A, 102, 15545–50. [PubMed: 16199517]

TOPALIAN SL, HODI FS, BRAHMER JR, GETTINGER SN, SMITH DC, MCDERMOTT DF, POWDERLY JD, CARVAJAL RD, SOSMAN JA, ATKINS MB, LEMING PD, SPIGEL DR, ANTONIA SJ, HORN L, DRAKE CG, PARDOLL DM, CHEN L, SHARFMAN WH, ANDERS RA, TAUBE JM, MCMILLER TL, XU H, KORMAN AJ, JURE-KUNKEL M, AGRAWAL S, MCDONALD D, KOLLIA GD, GUPTA A, WIGGINTON JM & SZNOL M 2012 Safety, activity, and immune correlates of anti-PD-1 antibody in cancer. The New England journal of medicine, 366, 2443–2454. [PubMed: 22658127]

VAN SCHALKWYK MC, PAPA SE, JEANNON JP, GUERRERO URBANO T, SPICER JF & MAHER J 2013 Design of a phase I clinical trial to evaluate intratumoral delivery of ErbB-targeted chimeric antigen receptor T-cells in locally advanced or recurrent head and neck cancer. Hum Gene Ther Clin Dev, 24, 134–42. [PubMed: 24099518]

VAREMO L, NIELSEN J & NOOKAEW I 2013 Enriching the gene set analysis of genome-wide data by incorporating directionality of gene expression and combining statistical hypotheses and methods. Nucleic Acids Res, 41, 4378–91. [PubMed: 23444143]

WANG X, CHANG W-C, WONG CW, COLCHER D, SHERMAN M, OSTBERG JR, FORMAN SJ, RIDDELL SR & JENSEN MC 2011 A transgene-encoded cell surface polypeptide for selection, in vivo tracking, and ablation of engineered cells. Blood, 118, 1255–1263. [PubMed: 21653320]

WHILDING LM, HALIM L, DRAPER B, PARENTE-PEREIRA AC, ZABINSKI T, DAVIES DM & MAHER J 2019 CAR T-Cells Targeting the Integrin alphavbeta6 and Co-Expressing the Chemokine Receptor CXCR2 Demonstrate Enhanced Homing and Efficacy against Several Solid Malignancies. Cancers (Basel), 11.

WOLOCK SL, LOPEZ R & KLEIN AM 2019 Scrublet: Computational Identification of Cell Doublets in Single-Cell Transcriptomic Data. Cell Syst, 8, 281–291 e9. [PubMed: 30954476]

WOO SR, FUERTES MB, CORRALES L, SPRANGER S, FURDYNA MJ, LEUNG MY, DUGGAN R, WANG Y, BARBER GN, FITZGERALD KA, ALEGRE ML & GAJEWSKI TF 2014 STING-dependent cytosolic DNA sensing mediates innate immune recognition of immunogenic tumors. Immunity, 41, 830–42. [PubMed: 25517615]

YAM PY, LI S, WU J, HU J, ZAIA JA & YEE JK 2002 Design of HIV vectors for efficient gene delivery into human hematopoietic cells. Mol Ther, 5, 479–84. [PubMed: 11945076]

YANG J, BASKAR S, KWONG KY, KENNEDY MG, WIESTNER A & RADER C 2011 Therapeutic potential and challenges of targeting receptor tyrosine kinase ROR1 with monoclonal antibodies in B-cell malignancies. PloS one, 6, e21018. [PubMed: 21698301]

ZILIONIS R, ENGBLOM C, PFIRSCHKE C, SAVOVA V, ZEMMOUR D, SAATCIOGLU HD, KRISHNAN I, MARONI G, MEYEROVITZ CV, KERWIN CM, CHOI S, RICHARDS WG, DE RIENZO A, TENEN DG, BUENO R, LEVANTINI E, PITTET MJ & KLEIN AM 2019 Single-Cell Transcriptomics of Human and Mouse Lung Cancers Reveals Conserved Myeloid Populations across Individuals and Species. Immunity, 50, 1317–1334 e10. [PubMed: 30979687]

Highlights

- ROR1 CAR-T cells infiltrate breast and lung tumors poorly and became dysfunctional
- Oxaliplatin (Ox) activates TAMs to express chemokines recruiting CAR-T cells
- CAR-T cells remodel the tumor microenvironment to amplify recruitment of T cells
- Ox improves CAR-T cell infiltration, tumor response to anti-PD-L1, and survival

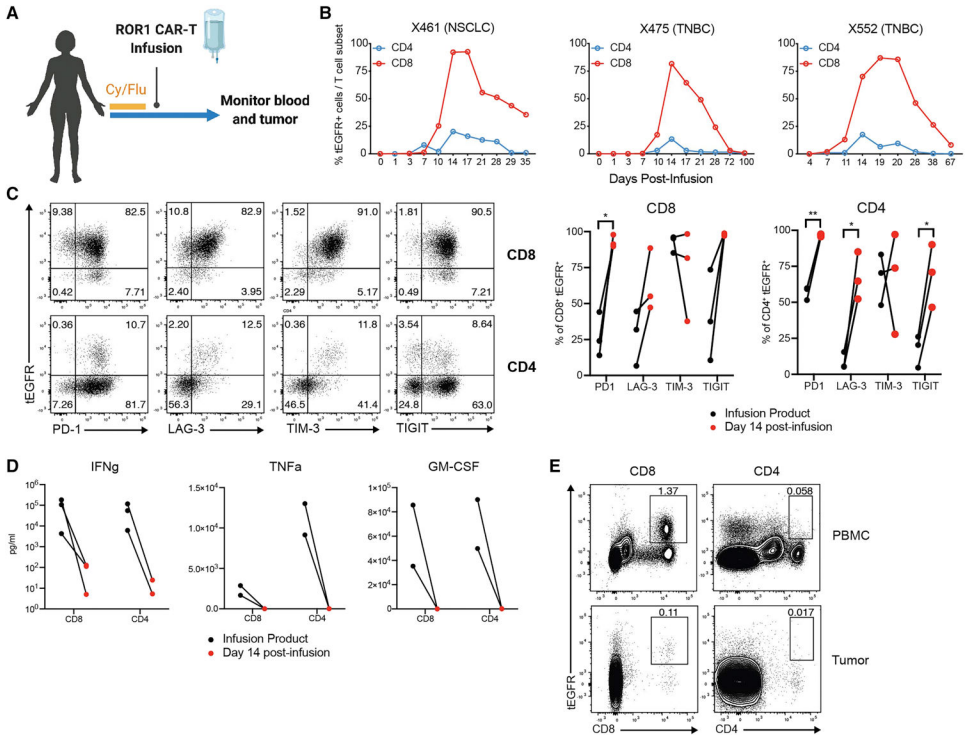

Figure 1. ROR1 CAR-T cells infiltrate tumors poorly and become dysfunctional in patients with ROR1$^+$ TNBC and NSCLC.

A) Treatment scheme. Cy=cyclophosphamide. Flu=fludarabine. B) Frequency of tEGFR$^+$ ROR1 CAR-T among total CD8$^+$ or CD4$^+$ T cells in blood of ROR1$^+$ TNBC or NSCLC patients. C) Left: flow analysis of tEGFR and inhibitory receptor expression on CD8$^+$ and CD4$^+$ T cells in blood of patient X552. Right: summary of inhibitory receptor expression on CD8$^+$tEGFR$^+$ and CD4$^+$tEGFR$^+$ CAR-T cells in blood of patients in (B) day 14 post-transfer relative to infusion product (IP). N=3 per group. Paired Student's two-way t-test. D) Luminex analysis of cytokine secretion by CD8$^+$tEGFR$^+$ and CD4$^+$tEGFR$^+$ ROR1 CAR-T cells from IP or blood of patients 14 days post-transfer after re-stimulation *ex vivo* with anti-CD3/CD28. N=2–3 per group. E) Flow analysis of live cells from PBMC and tumor 21 days post-infusion from patient X475. See also Table S1.

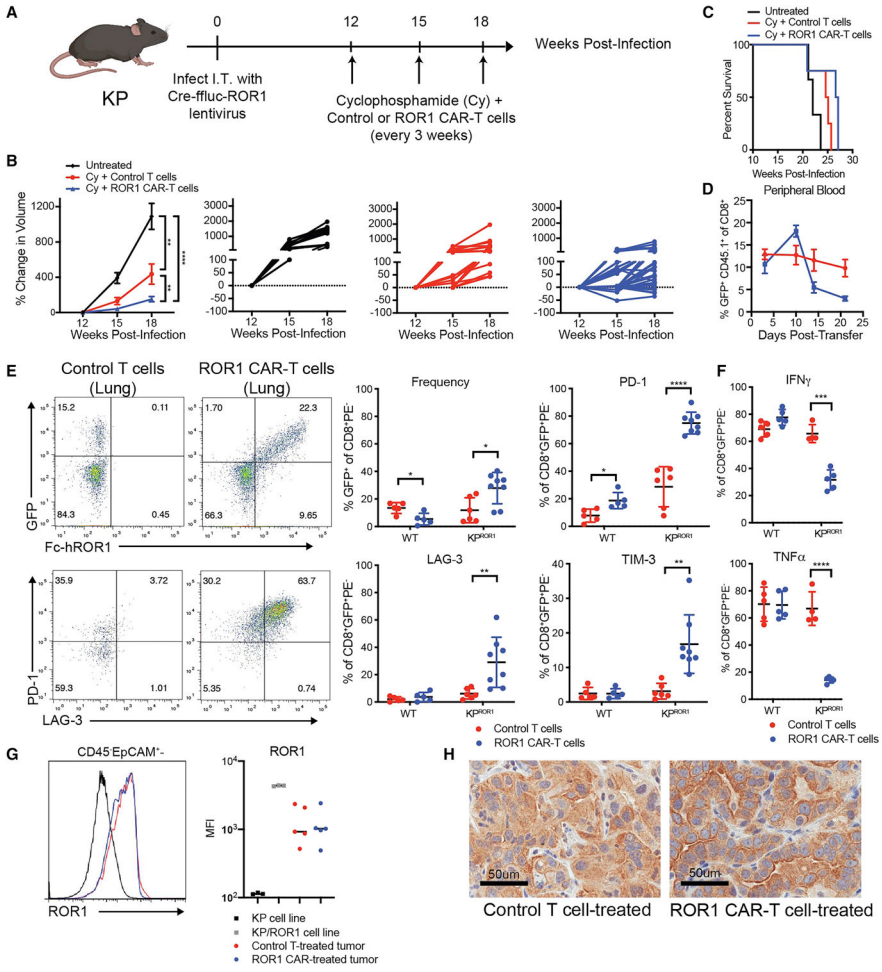

Figure 2. ROR1 CAR-T cells modestly control tumor growth in KP^{ROR1} mice.

A) Treatment scheme. I.T.=intratracheally. Ffluc=firefly luciferase. B) Percent change in total tumor (left) or individual tumor volume (right) quantified by MRI in KP^{ROR1} mice. N=3–4 mice per group. Two-way ANOVA with Tukey's post-test. C) Survival of KP^{ROR1} mice. N=3–4 mice per group. Log-rank Mantel-Cox test. D) Frequency of CD45.1^{+}CD8^{+}GFP^{+} control (red) or CAR-T cells (blue) in blood. N=6–8 mice per group. E) Left: flow analysis of GFP and Fc-ROR1 (CAR) expression on PE^{-}CD8^{+} non-vascular T cells (top) and PD-1 and LAG-3 expression on PE^{-}CD8^{+}GFP^{+} non-vascular control or CAR-T cells (bottom) from lungs of KP^{ROR1} mice 10 days post-transfer. Right: Summary of PE^{-} control and CAR-T cell frequency and inhibitory receptor expression in WT or KP^{ROR1} lungs 10 days post-transfer. N=6–8 mice per group. Unpaired Student's two-way t-test. F) Intracellular cytokine analysis in CD45.1^{+}CD8^{+}GFP^{+} control (red) or CAR-T cells (blue) from lungs of WT or KP^{ROR1} mice 10 days post-transfer and re-stimulated with PMA/ionomycin. N=5 mice per group. Student's unpaired two-way t-test. G) Flow analysis of hROR1 expression on primary CD45^{-}EpCAM^{+} lung epithelial cells from control or CAR-T cell-treated KP^{ROR1} mice 10 weeks post-transfer or on KP cell lines overexpressing hROR1. N=5 mice per group. H) ROR1 IHC staining on control or CAR-T cell-treated KP^{ROR1} lungs 10 weeks post-transfer. Data are representative of 4 independent experiments. See also Figures S1–S3.

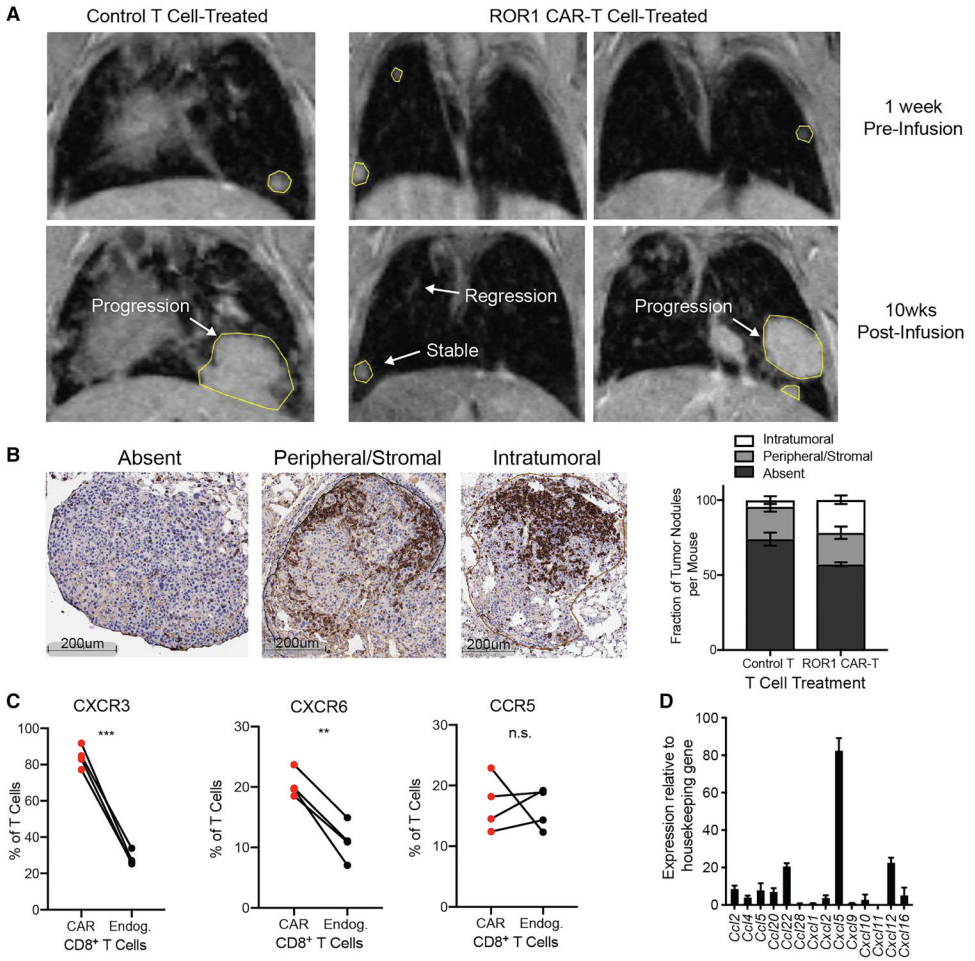

Figure 3. ROR1 CAR-T cells do not efficiently infiltrate all KP^{ROR1} tumors.

A) Representative MRI scans of KP^{ROR1} mice treated as indicated. B) Left: CD3 IHC staining showing T cell localization patterns. Right: percentage of individual tumors per mouse with indicated T cell localization pattern in control- and CAR-T cell-treated KP^{ROR1} mice. N=4 mice per group. C) Flow analysis of chemokine receptor expression on CD45.1^{+}CD8^{+}GFP^{+} CAR-T cells or CD45.2^{+}CD8^{+} endogenous T cells in blood of KP^{ROR1} mice 3 days post-transfer. N=4 mice per group. Paired Student's two-way t-test. D) qPCR of chemokines relative to housekeeping genes in untreated KP^{ROR1} tumors 13 weeks post-infection. N=4 mice per group. Data are representative of 2 independent experiments.

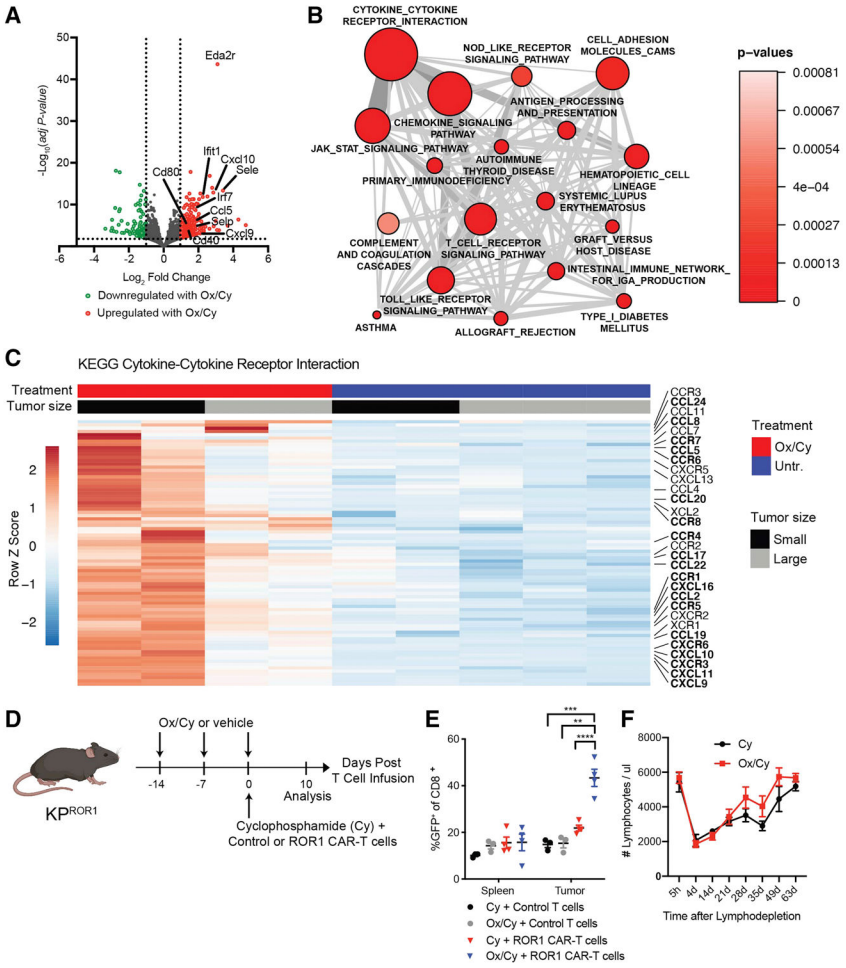

Figure 4. Ox/Cy enhances chemokine expression and CAR-T cell accumulation in KP^{ROR1} tumors.

A) Volcano plot of genes significantly upregulated (red) or downregulated (green) in tumors excised and pooled from Ox/Cy-treated or untreated KP^{ROR1} mice, 6 hours post-Ox/Cy injection. N=4–5 mice per group. B) Network plot of top KEGG pathways enriched among genes upregulated by Ox/Cy. Node size is proportional to number of genes within each gene set; thickness of grey line between nodes indicates proportion of shared genes between genesets. C) Heatmap of leading-edge genes in “Cytokine-Cytokine Receptor Interaction” pathway. Genes encoding chemokines are highlighted, with those involved in T cell recruitment indicated in bold. D) Treatment scheme. E) Frequency of CD45.1^{+}CD8^{+}GFP^{+} control and CAR-T cells in spleens and tumors excised and pooled from KP^{ROR1} mice 10 days post-transfer. N=4 mice per group. One-way ANOVA with Tukey’s post-test. F) Lymphocyte counts in peripheral blood of KP^{ROR1} mice treated with Cy or Ox/Cy. N=4 mice per group. Data are representative of 2 independent experiments.

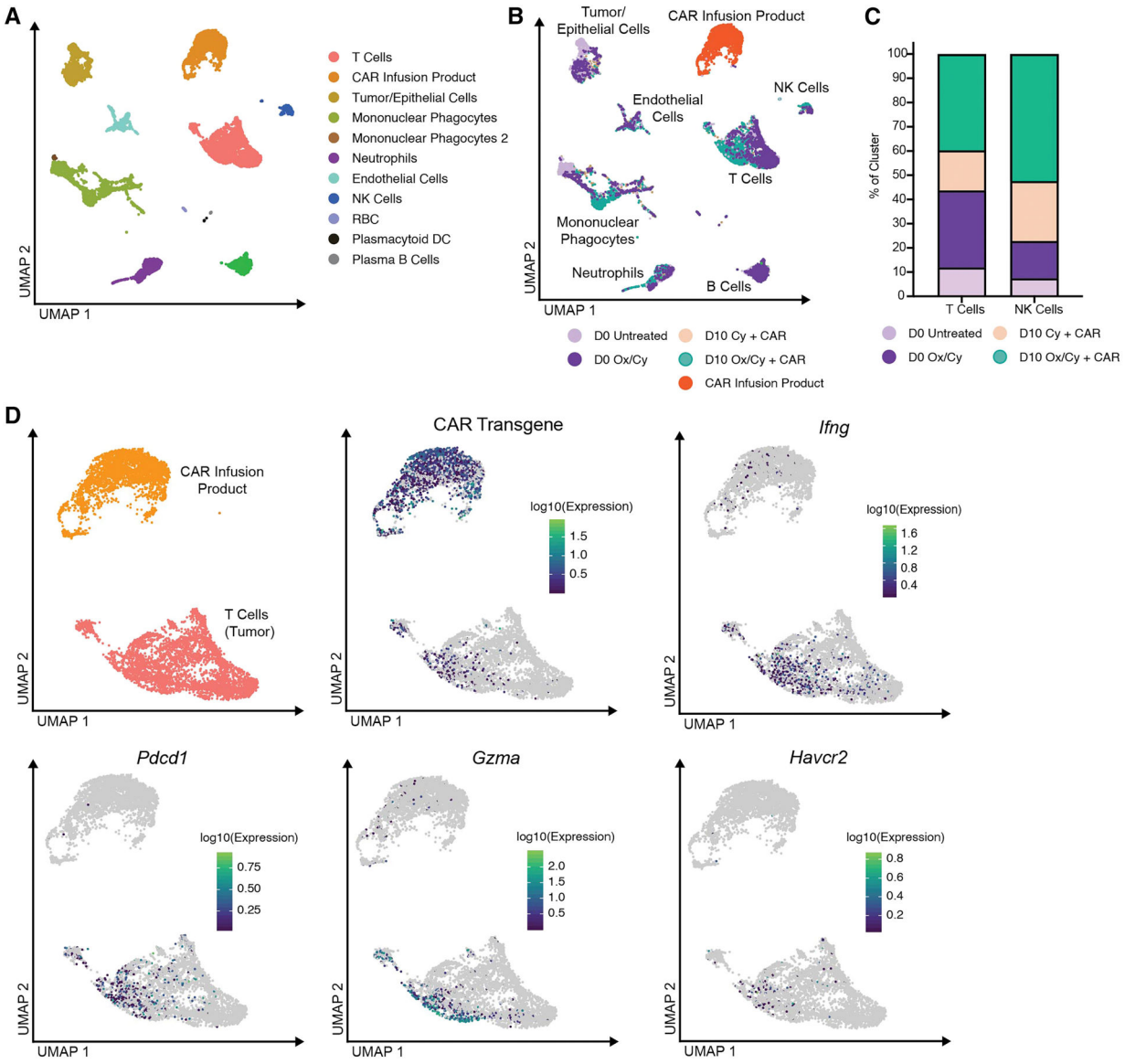

Figure 5. Ox/Cy enhances accumulation of tumor-infiltrating CAR-T cells with an activated phenotype.

A) Unsupervised clustering of cells derived from tumors excised and pooled from untreated (day 0), Ox/Cy-treated (day 0, 6 hours post-Ox/Cy), Cy + CAR-T cell-treated (day 10), and Ox/Cy + CAR-T cell-treated (day 10) KP^{ROR1} mice and analyzed by scRNA-seq. B) Clusters in (A) colored by tumor sample type. C) Percent of indicated clusters comprised of indicated tumor sample. D) Expression of indicated genes in CAR-T cell infusion product and tumor-infiltrating T cell clusters. See also Figures S4 and S5.

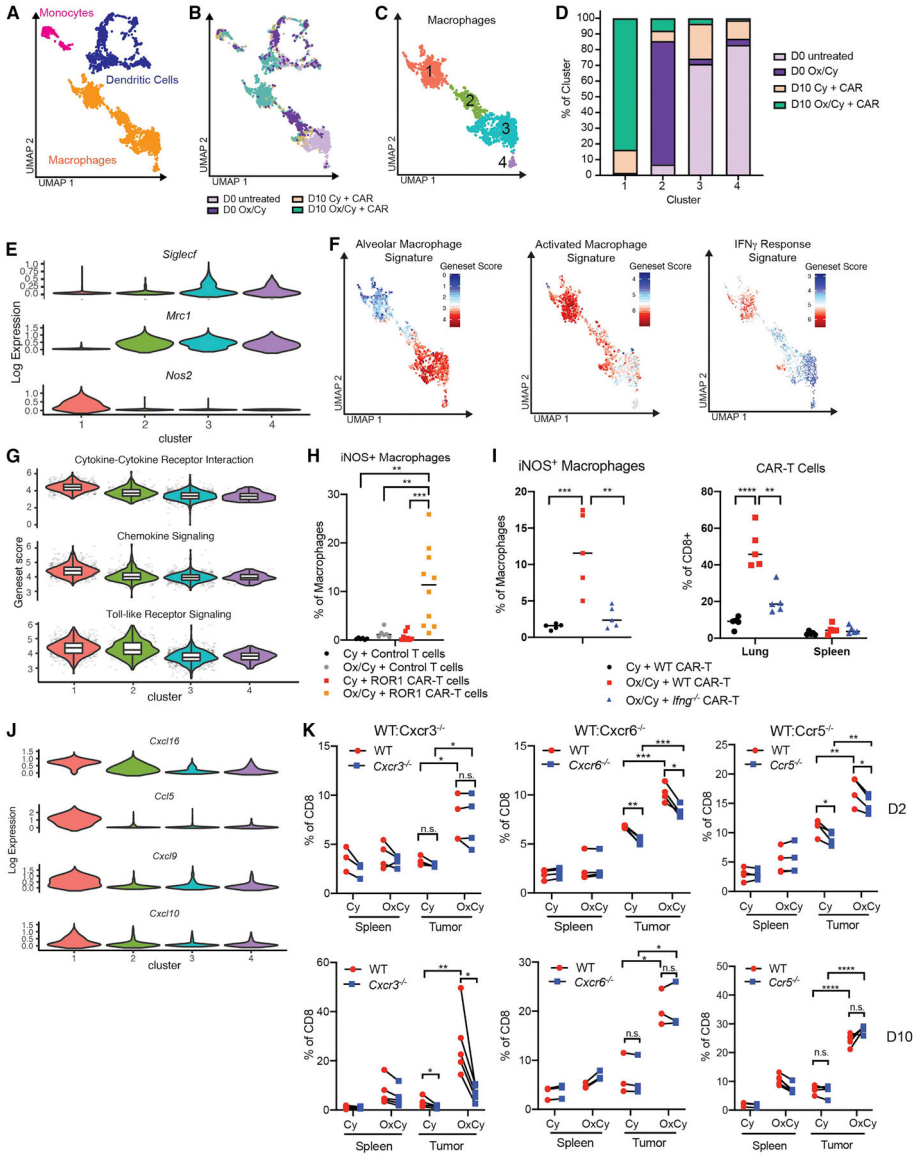

Figure 6. Ox/Cy activates expression of T cell-recruiting chemokines by tumor macrophages.

A) Unsupervised clustering of mononuclear phagocyte (MNP) cluster from Fig. 5A. B) MNP clusters in (A) colored by tumor sample type. C) Unsupervised clustering of macrophage cluster in (A). D) Fraction of macrophage cluster comprised of each tumor sample type. E) Violin plots of select genes in macrophage sub-clusters. F) Geneset scores of enriched pathways in macrophage sub-clusters. G) Violin plots of geneset score of indicated KEGG pathways in macrophage sub-clusters. H) Frequency of iNOS$^+$ cells among F4/80$^+$ macrophages in tumors excised and pooled from KP^{ROR1} mice 10 days after treatment. N=6–10 mice per group. One-way ANOVA with Tukey's post-test. I) Frequency of iNOS$^+$ cells among F4/80$^+$ macrophages (left) and CAR-T cells among CD8$^+$ T cells (right) in spleens and tumors excised and pooled from KP^{ROR1} mice 10 days after treatment. N=5 mice per group. One-way ANOVA with Tukey's post-test. J) Violin plots of chemokine expression in macrophage sub-clusters. K) Frequency of WT (red) and chemokine receptor

knockout (blue) CAR-T cells in tumors excised and pooled from Ox/Cy- or vehicle-treated KP^{ROR1} mice 2 days (top) or 10 days (bottom) after transfer. N=3–4 mice per group. Paired Student's two-way t-test. Data in 6H, 6I, and 6K are representative of 2–3 independent experiments. See also Figure S6.

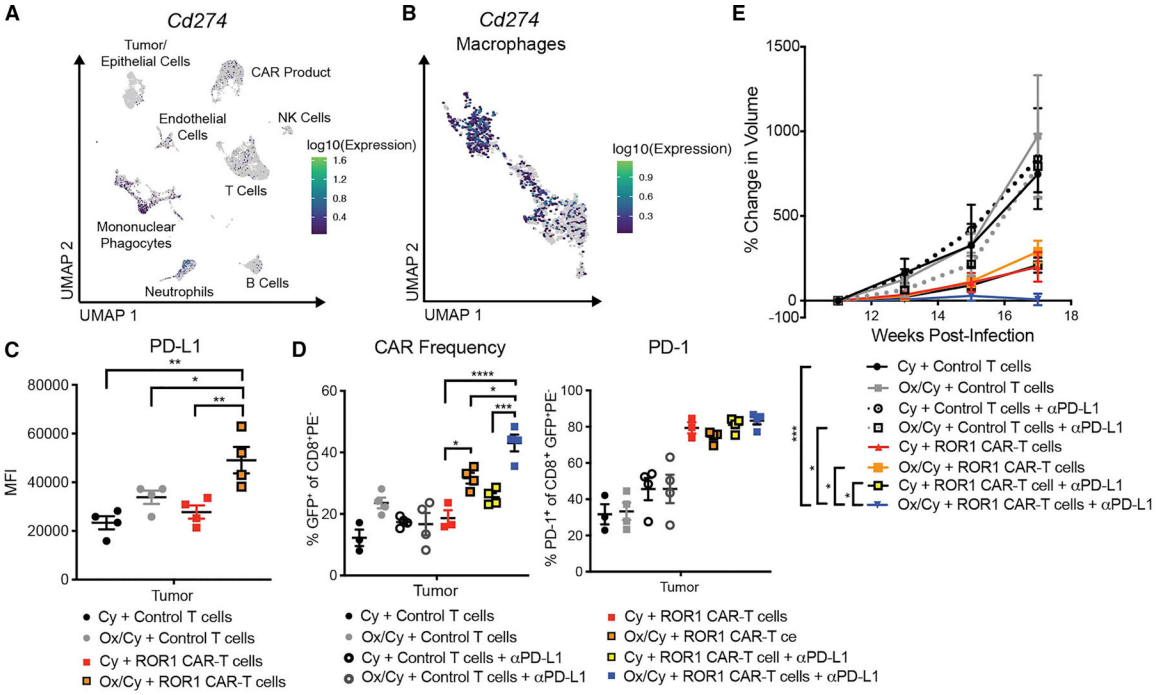

Figure 7. Ox/Cy-enhanced CAR-T cell infiltration sensitizes tumors to anti-PD-L1.

A, B) Expression of *Cd274* among scRNA-seq clusters from Fig. 5A (A) and macrophage subclusters from Fig. 6A (B). C) Median fluorescence intensity of PD-L1 on F4/80^{+} macrophages in lungs from KP^{ROR1} mice 10 days after treatment. N=4 mice per group. One-way ANOVA with Tukey's post-test. D) Frequency and PD-1 expression on CD45.1^{+}CD8^{+}GFP^{+}PE^{-} transferred control or CAR-T cells in lungs of KP^{ROR1} mice treated as indicated 10 days after the second infusion of T cells. N=4 mice per group. One-way ANOVA with Tukey's post-test. E) Percent change in tumor volume in KP^{ROR1} mice treated as indicated. N=4 mice per group. Two-way ANOVA with Tukey's post-test. Data are representative of 2 independent experiments.

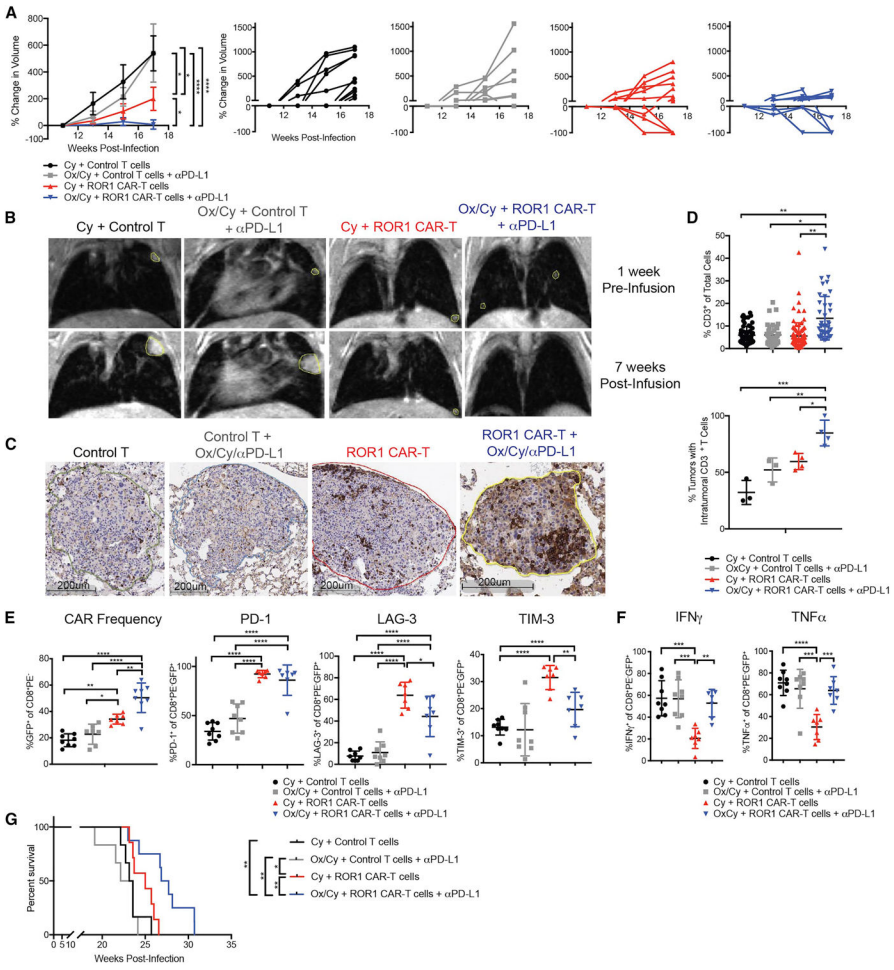

Figure 8. Ox/Cy and anti-PD-L1 improve CAR-T cell-mediated tumor control and survival.

A) Percent change in total (left) or individual tumor volume (right) in KP^{ROR1} mice treated as indicated. N=4 mice per group. Two-way ANOVA with Tukey's post-test. B) Representative MRI scans of KP^{ROR1} mice. C) CD3 IHC staining on lungs from KP^{ROR1} mice 10 days after the second infusion of T cells. D) Quantification of CD3^{+} T cells in individual KP^{ROR1} tumor nodules and fraction of tumors in each mouse showing intratumoral localization. N=4 mice per group. One-way ANOVA with Tukey's post-test. E) Flow analysis of CD45.1^{+}CD8^{+}GFP^{+}PE^{-} control and CAR-T cells in lungs of KP^{ROR1} mice 10 days after the second infusion of T cells. N=7–8 mice per group. One-way ANOVA with Tukey's post-test. F) Intracellular cytokine analysis of CD45.1^{+}CD8^{+}GFP^{+}PE^{-} control and CAR-T cells isolated from lungs of KP^{ROR1} mice 10 days after the second infusion of T cells and re-stimulated with PMA/ionomycin. N=7–8 mice per group. One-way ANOVA with Tukey's post-test. G) Survival of KP^{ROR1} mice. N=6–8 mice per group. Log-rank Mantel-Cox test. A-F: Data are representative of two independent experiments. G: Data are combined from two independent experiments. See also Figures S7 and S8.

KEY RESOURCES TABLE

REAGENT or RESOURCE	SOURCE	IDENTIFIER
Antibodies		
Anti-mouse CD4 PerCP-Cy5.5	BioLegend	Cat# 116012 RRID: AB_2563023
Anti-mouse CD4 APC-ef780	Thermo Fisher	Cat# 47-0041-82 RRID: AB_11218896
Anti-mouse CD4 BV785	BioLegend	Cat# 100552 RRID: AB_2563053
Anti-mouse CD8 APC-eFluor780	Thermo Fisher	Cat# 9047-0087-120 RRID:AB_11181660
Anti-mouse CD8 BUV395	BD Biosciences	Cat# 563786, RRID:AB_2732919
Anti-mouse CD45.1 Pacific Blue	BioLegend	Cat# 110722, RRID:AB_492866
Anti-mouse CD45.1 APC-ef780	Thermo Fisher	Cat# 47-0453-82 RRID: AB_158222
Anti-mouse CD90.2 FITC	BioLegend	Cat# 140303 RRID:AB_10642686
Anti-mouse CD3 FITC	BioLegend	Cat# 100306, RRID:AB_312671
Anti-mouse CD19 FITC	Thermo Fisher	Cat# 11-0193-82 RRID:AB_657666
Anti-mouse NK1.1 FITC	BioLegend	Cat# 108706 RRID:AB_313393
Anti-mouse NKp46 FITC	BioLegend	Cat# 137606 RRID:AB_2298210
Anti-mouse B220 FITC	BioLegend	Cat# 103206, RRID:AB_312991
Anti-mouse CD45.2 APC-ef780	BioLegend	Cat#109820 RRID:AB_492872
Anti-mouse PD-1 PECy7	BioLegend	Cat# 135216, RRID: AB_10689635
Anti-mouse PD-1 BV605	BioLegend	Cat# 135220, RRID:AB_2562616
Anti-mouse LAG-3 BV785	BioLegend	Cat#125219 RRID:AB_2566571
Anti-mouse TIM-3 APC	BioLegend	Cat# 119705 RRID: AB_2561655
Anti-mouse CXCR3 APC	BioLegend	Cat#126536 RRID:AB_2566565
Anti-mouse CXCR6 PE	BioLegend	Cat# 151104 RRID:AB_2566546
Anti-mouse CCR5 PE	BioLegend	Cat# 107012 RRID:AB_2074527
Anti-mouse CD25 PE-e610	Thermo Fisher	Cat# 61-0251-82 RRID:AB_2574542
Anti-mouse CD44 BV605	BioLegend	Cat# 103047 RRID:AB_2562451
Anti-mouse CD69 BV421	BioLegend	Cat# 104527 RRID:AB_10900250
Anti-mouse TIGIT PECy7	BioLegend	Cat# 142107 RRID:AB_2565648

REAGENT or RESOURCE	SOURCE	IDENTIFIER
Anti-mouse CD11b BV605	BioLegend	Cat#101237 RRID:AB_11126744
Anti-mouse CD11c Pacific Blue	BioLegend	Cat# 117322 RRID:AB_755988
Anti-mouse Ly6C APC-ef780	Thermo Fisher	Cat# 47-5932-80 RRID:N/A
Anti-mouse Ly6G BUV395	BD Biosciences	Cat# 563978 RRID:AB_2716852
Anti-mouse F4/80 BV785	BioLegend	Cat# 123141 RRID:AB_2563667
Anti-mouse I-A/I-E AlexaFluor700	BioLegend	Cat#107622 RRID:AB_493727
Anti-mouse CD24 BUV496	BD Biosciences	Cat# 612953 RRID: N/A
Anti-mouse CD64 PECy7	BioLegend	Cat# 139314 RRID:AB_2563904
Anti-mouse SiglecF PerCP-Cy5.5	BD Biosciences	Cat# 565526 RRID:AB_2739281
Anti-mouse PD-L1 BV421	BioLegend	Cat# 124315 RRID:AB_10897097
Anti-mouse EpCAM PECy7	Thermo Fisher	Cat# 118216 RRID:AB_1236471
Anti-human ROR1 APC	Miltenyi Biotec	Cat# 130-117-942, RRID:AB_2733449
Anti-human IgG BV421	BioLegend	Cat# 409318 RRID:AB_2562176
Fc-ROR1 purified	FHCRC Protein Core	N/A
Anti-mouse IFNg PECy7	BioLegend	Cat# 505826 RRID:AB_2295770
Anti-mouse TNFa Pacific Blue	Thermo Fisher	Cat# 48-7321-82 RRID:AB_1548825
Anti-mouse Foxp3 PECy7	Thermo Fisher	Cat# 25-5773-82 RRID:AB_891552
Anti-mouse/human Ki-67 AlexaFluor700	BD Biosciences	Cat# 561277 RRID:AB_10611571
Anti-mouse CTLA-4 PE-e610	Thermo Fisher	Cat# 61-1522-82 RRID:AB_2574581
Anti-mouse CD206 PE	BioLegend	Cat# 141706 RRID:AB_10895754
Anti-mouse iNOS APC	Thermo Fisher	Cat# 17-5920-82 RRID:AB_2573244
Anti-mouse CD45 BUV805	BD Biosciences	Cat# 748370
Anti-mouse CD45 PE	BioLegend	Cat #103106 RRID:AB_312971
Live/Dead Fixable Aqua Cell Stain Kit	Thermo Fisher	Cat# L34957
Fixable Viability Dye eFluor506	Thermo Fisher	Cat# 65-0866-14
Anti-human EGFR biotin	FHCRC, Riddell lab	N/A
Streptavidin APC	Thermo Fisher	Cat# 17-4317-82
Anti-human CD3 Pacific Blue	BD Biosciences	Cat# 558117 RRID: AB_397038

REAGENT or RESOURCE	SOURCE	IDENTIFIER
Anti-human CD4 PerCPCy5.5	BioLegend	Cat# 300530 RRID:AB_893322
Anti-human CD8 AlexaFluor 700	BioLegend	Cat# 344724 RRID:AB_2562790
Anti-human CD8 FITC	BioLegend	Cat# 300906 RRID:AB_314110
Anti-human CD45 PerCPCy5.5	BD Biosciences	Cat# 564105
Anti-human PD-1 PE	Thermo Fisher	Cat# 12-2799-42 RRID:AB_11042478
Anti-human TIM-3 PE	BioLegend	Cat# 345006 RRID: AB_2116576
Anti-human LAG-3 PE	Thermo Fisher	Cat# 12-2239-42 RRID:AB_2572597
Anti-human TIGIT PE	Thermo Fisher	Cat# 12-9500-42 RRID:AB_10714831
Mouse IgG1 k isotype PE	BioLegend	Cat# 400112 RRID:AB_2847829
Anti-mouse CD3e purified	BD Biosciences	Cat #553057 RRID:AB_394590
Anti-mouse CD28 purified	BD Biosciences	Cat #553294 RRID:AB_394763
Anti-mouse PD-L1	Bio X Cell	Cat #BE0101 RRID:AB_10949073
Anti-human CD3, purified	BioLegend	Cat #317302 RRID:AB_571927
Anti-human CD28, purified	BioLegend	Cat #302902 RRID:AB_314304
Anti-CD3	Serotec	Cat #MCA1477 RRID:AB_321245
Anti-ROR1	Cell Signaling Technologies	Cat #4102 RRID:AB_2180136
Rabbit anti-rat secondary	Rockland	Cat #712-4126 RRID:AB_217723
Chemicals, Peptides, and Recombinant Proteins		
Mouse T-Activator CD3/28 Dynabeads	Thermo Fisher	Cat #11452D
Human T-Activator CD3/28 Dynabeads	Thermo Fisher	Cat #11132D
Retronectin	Takara	Cat #T202
Cyclophosphamide	Baxter (SCCA Pharmacy)	N/A
Oxaliplatin	Hospira (SCCA Pharmacy)	N/A
Critical Commercial Assays		
EasySep Human CD8+ T Cell Isolation Kit	Stem Cell Technologies	Cat #17953
EasySep Human CD4+ T Cell Isolation Kit	Stem Cell Technologies	Cat #17952
EasySep Mouse CD8+ T Cell Isolation Kit	Stem Cell Technologies	Cat #19853
EasySep Mouse CD4+ T Cell Isolation Kit	Stem Cell Technologies	Cat #19852
CD19 Microbeads, Mouse	Miltenyi Biotec	Cat #130-121-301 RRID:AB_2827612
Tumor Dissociation Kit, Mouse	Miltenyi Biotec	Cat #130-096-730

REAGENT or RESOURCE	SOURCE	IDENTIFIER
RNeasy Mini kit	QIAGEN	Cat #74134
RT2 First Strand Kit	QIAGEN	Cat #330404
RT2 Profiler PCR Array Mouse Cancer Inflammation & Immunity Crosstalk	QIAGEN	Cat #PAMM-181Z
10X Genomics 3' Chromium v2.0	10X Genomics	PN-120237; PN-120236; PN-120262
Deposited Data		
Bulk RNAseq data	This paper	GEO: GSE158111
Single cell RNAseq data	This paper	GEO: GSE158111
Experimental Models: Cell Lines		
KP1233	Tyler Jacks (MIT)	N/A
3TZ "GreenGo"	Tyler Jacks (MIT)	N/A
4T1	ATCC	Cat# CRL-2539, RRID:CVCL_0125)
Lenti-X 293T	Clontech	Cat #632180
Plat-E	Cell Biolabs	RRID:CVCL_B488
MDA-MB-231	ATCC	Cat# HTB-26, RRID:CVCL_0062
Experimental Models: Organisms/Strains		
Mouse: C57BL/6 (B6): C57BL/6J	The Jackson Laboratory	Cat# JAX:000664, RRID:IMSR_JAX:000664
Mouse: B6 CD45.1: B6.SJL-*Ptprc*^{a} *Pepc*^{b}/BoyJ	The Jackson Laboratory	Cat# JAX:002014, RRID:IMSR_JAX:002014
Mouse: BALB/c: BALB/cByJ	The Jackson Laboratory	Cat# JAX:001026, RRID:IMSR_JAX:001026
Mouse: B6 *Cxcr3*$^{-/-}$: B6.129P2-*Cxcr3*^{tm1Dgen}/*J*	The Jackson Laboratory	Cat# JAX:005796, RRID:IMSR_JAX:005796
Mouse: B6 *Cxcr6*$^{-/-}$: B6.129P2-*Cxcr6*^{tm1Litt}/*J*	The Jackson Laboratory	Cat# JAX:005693, RRID:IMSR_JAX:005693
Mouse: B6 *Ccr5*$^{-/-}$: B6.129P2-*Ccr5*^{tm1Kuz}/*J*	The Jackson Laboratory	Cat# JAX:005427, RRID:IMSR_JAX:005427
Mouse: B6 *Ifng*$^{-/-}$: B6.129S7-*Ifng*^{tm1Ts}/J	The Jackson Laboratory	Cat# JAX:002287 RRID:IMSR_JAX:002287
Mouse: Kras$^{LSL\text{-}G12D/+}$;p53$^{f/f}$	A. McGarry Houghton (FHCRC, Seattle WA)	Cat# JAX:032435, RRID:IMSR_JAX:032435
Oligonucleotides		
mCxcl16 F primer: 5'-AAAGAGTGTGGAACTGGTCATG-3'	This paper	N/A
mCxcl16 R primer: 5'-AGCTGGTGTGCTAGCTCCAG −3'	This paper	N/A
mActb F primer: 5'-CTGTCCCTGTATGCCTCTG-3'	This paper	N/A
mActb R primer: 5'-ATGTCACGCACGATTTCC-3'	This paper	N/A
Recombinant DNA		
Plasmid: pMP71_2A2_IgG4sh_mCD28TM_m41BB_mCD3z_P2A_tCD19	This paper	N/A
Plasmid: pMP71_tCD19	This paper	N/A
Plasmid: pMP71_2A2_IgG4sh_mCD28TM_m41BB_mCD3z_P2A_tCD19-GFP	This paper	N/A
Plasmid: pMP71_tCD19-GFP	This paper	N/A

REAGENT or RESOURCE	SOURCE	IDENTIFIER
Plasmid: epHIV7_Cre_P2A_ffluc	This paper	N/A
Plasmid: epHIV7_Cre_P2A_ffluc_T2A_hROR1t	This paper	N/A
Plasmid: psPax2	Addgene	Addgene Plasmid #12260
Plasmid: pMD2.G (VSVg)	Addgene	Addgene Plasmid #12259
Software and Algorithms		
FlowJo v10	TreeStar	https://www.flowjo.com/solutions/flowjo/downloads
Prism	GraphPad	https://www.graphpad.com/scientific-software/prism/
HALO Image Analysis Software	Indica Labs	http://www.indicalab.com/halo/
Living Image Software	Perkin Elmer	http://www.perkinelmer.com/product/li-software-for-spectrum-1-seat-add-on-128113
VivoQuant	Invicro	http://www.vivoquant.com/
Other		
Power SYBR Green PCR Master Mix	Thermo Fisher	Cat #4367659